

On the Spatial Distribution of ^{13}CO Structures within ^{12}CO Molecular Clouds

LIXIA YUAN ¹, JI YANG ¹, FUJUN DU ¹, XUNCHUAN LIU ², YANG SU ¹, QING-ZENG YAN ¹, XUEPENG CHEN,¹
YAN SUN ¹, SHAOBO ZHANG ¹, XIN ZHOU ¹ AND YUEHUI MA ¹

¹*Purple Mountain Observatory and Key Laboratory of Radio Astronomy, Chinese Academy of Sciences,
10 Yuanhua Road, Qixia District, Nanjing 210033, PR China*

²*Shanghai Astronomical Observatory, Chinese Academy of Sciences, PR China*

ABSTRACT

We look into the 2851 ^{12}CO molecular clouds harboring ^{13}CO structures to reveal the distribution of the projected angular separations and radial velocity separations between their internal ^{13}CO structures. The projected angular separations are determined using the minimal spanning tree algorithm. We find that $\sim 50\%$ of the angular separations fall in a narrow range of $\sim 3 - 7$ arcmin with a median of ~ 5 arcmin, and the corresponding radial velocity separations mainly range from $\sim 0.3 \text{ km s}^{-1}$ to 2.5 km s^{-1} . The mean and standard deviation of the angular separations of the internal ^{13}CO structures within ^{12}CO clouds appear to be universal, independent of the ^{12}CO cloud angular areas and the counts of their internal ^{13}CO structures. We also reveal a scaling relation between the ^{12}CO cloud angular area and its harbored ^{13}CO structure count. These results suggest there is a preferred angular separation between ^{13}CO structures in these ^{12}CO clouds, considering the distance effects. According to that, we propose an alternative picture for the assembly and destruction of molecular clouds: there is a fundamental separation for the internal structures of molecular clouds, the build-up and destruction of molecular clouds proceeds under this fundamental unit.

Keywords: Interstellar medium(847) — Interstellar molecules(849) — Molecular clouds(1072)

1. INTRODUCTION

Molecular clouds (MCs) are the densest ($n > 30 \text{ cm}^{-3}$), darkest, and coldest ($\sim 10 \text{ K} - 20 \text{ K}$) molecular phase of the interstellar medium (ISM). They are linked with star formation, planet formation, and galaxy evolution. Hence it is essential to understand the nature of MCs, passing through an understanding on their hierarchical structures, physical properties, and dynamics. Several typical mechanisms on the formation and evolution of MCs have been proposed, including large-scale gravitational instabilities (Lin & Shu 1964; Goldreich & Lynden-Bell 1965), turbulent flows (Vazquez-Semadeni et al. 1995; Passot et al. 1995; Ballesteros-Paredes et al. 1999a; Vázquez-Semadeni et al. 2006; Heitsch et al. 2006; Beuther et al. 2020), and agglomeration of smaller clouds (Oort 1954; Field & Saslaw 1965; Dobbs & Baba 2014), however many questions are still

open. For instance, giant molecular clouds usually exhibit complex and hierarchical structures, inside which smaller and denser structures or clumps are found at different levels of the hierarchy, it is still not clear that how these internal substructures and dense gas gather in MCs.

Filamentary structures are widespread in molecular clouds (André et al. 2010; Molinari et al. 2010). The filament populations have a wide range of properties in terms of lengths, aspect ratios, widths, and masses (Arzoumanian et al. 2011; Li et al. 2013; Hacar et al. 2013; Wang et al. 2016; Mattern et al. 2018; Hacar et al. 2018, 2022), they are also known to play an important role in star formation, considering the observed tendency of pre-stellar cores and young stellar objects (YSOs) to be associated with filaments (Myers 2009; Polychroni et al. 2013; Schisano et al. 2014; André et al. 2014, 2016; Könyves et al. 2015; Hacar et al. 2018; Könyves et al. 2020; Yuan et al. 2020). Our previous works in Yuan et al. (2021) (Paper I) classified 18,190 MCs, which were identified by ^{12}CO lines data from the Milky Way Imaging Scroll Painting (MWISP) survey (Su et al. 2019),

into filaments and nonfilaments (Yuan et al. 2021). In that work, it found that filaments making up $\sim 10\%$ of the total number, contribute $\sim 90\%$ of the total integrated fluxes of ^{12}CO line emission. In addition, Yuan et al. (2022) (Paper II) extracted ^{13}CO gas structures within each of 18,190 ^{12}CO clouds using the ^{13}CO lines from the MWISP survey. Among that, there are 2851 ^{12}CO clouds ($\sim 15\%$) having ^{13}CO gas structures. Combining the results from Paper I and II, we find that the MCs classified as filaments tend to have larger spatial areas and more substructures traced by ^{13}CO lines. However, what kind of a relation does exist between the spatial scales of ^{12}CO clouds and their internal ^{13}CO structures? Answering this question may help to understand how molecular gas gathers to form stars on its way from MCs to substructures.

Among the 2851 ^{12}CO MCs having ^{13}CO structures, $\sim 60\%$ of these ^{12}CO clouds have a single ^{13}CO structure, $\sim 15\%$ of them have double ^{13}CO structures, and the rest $\sim 20\%$ of them have multiple (more than two) ^{13}CO structures (Yuan et al. 2022). These results indicate the distribution of high-density gas in MCs is inhomogeneous. Using ^{13}CO line emission within ^{12}CO clouds, we have provided the high-density gas content in these ^{12}CO clouds (Yuan et al. 2022). However, the spatial distributions of the ^{13}CO structures within ^{12}CO clouds are still not well investigated. This information may provide essential clues to understand how the dense gas content and the internal sub-structures develop in the MCs, to reveal the building-up process of MCs.

In this paper, we aim to reveal the spatial distribution and the relative motion between the internal ^{13}CO structures within 2851 ^{12}CO clouds. Section 2 mainly describes the ^{12}CO and ^{13}CO lines data, the ^{12}CO molecular cloud samples, and their internal ^{13}CO structures. Section 3 presents the results, including the physical properties of these individual ^{13}CO structures, the distributions of the projected angular separations and radial velocity separations between ^{13}CO structures within these ^{12}CO clouds. Section 4 mainly discusses the observational effects on the observed ^{13}CO structure separations and also reveal the scaling relations between the internal ^{13}CO structures and their natal ^{12}CO clouds. We conclude in Section 5 with our results.

2. DATA

2.1. ^{12}CO and ^{13}CO lines data from MWISP survey

The MWISP survey is an ongoing northern Galactic plane CO survey, which utilizes the 13.7m telescope at Delingha, China, to observe the J= 1-0 transitions of the ^{12}CO , ^{13}CO , and C^{18}O lines, simultaneously. A detailed description of the survey is given in Su et al.

(2019). The typical noise temperature is ~ 250 K for ^{12}CO line and ~ 140 K for $^{13}\text{CO}/\text{C}^{18}\text{O}$ lines. The half-power beamwidth (HPBW) is about $50''$ at 115 GHz. The velocity resolution of ^{13}CO lines is about 0.17 km s^{-1} . An rms noise level of ~ 0.5 K for ^{12}CO lines and ~ 0.3 K for the ^{13}CO lines are achieved.

In this work, we focus on the ^{12}CO and ^{13}CO line emission in the second Galactic quadrant with $104^\circ.75 < l < 150^\circ.25$, $|b| < 5^\circ.25$, and -95 km $\text{s}^{-1} < V_{\text{LSR}} < 25$ km s^{-1} . The ^{12}CO and ^{13}CO lines emission data in this region have been published in paper I and II, respectively.

2.2. ^{12}CO molecular clouds and ^{13}CO structures

A catalog of 18,190 ^{12}CO molecular clouds has been identified from the ^{12}CO line emission in the above region, using the Density-based Spatial Clustering of Applications with Noise (DBSCAN) algorithm (Ester et al. 1996; Yan et al. 2021b). The DBSCAN algorithm extracts a set of contiguous voxels in the position-position-velocity (PPV) cube with ^{12}CO line intensities above a certain threshold as a molecular cloud. The line intensity threshold is determined by the parameter of ‘cutoff’. The connectivity of extracted structures is confined by two parameters of ϵ and MinPts. A core point within the extracted consecutive structure, whose adjacent points within a certain radius have to exceed a number threshold. The ‘MinPts’ determines the threshold of the number of adjacent points and ϵ determines the radius of the adjacency. The border points are the points inside the ϵ -neighborhood of core points, but do not contain the ‘MinPts’ neighbors in its ϵ -neighborhood (Ester et al. 1996). The parameters of cutoff = 2σ (σ is the rms noise, whose value is ~ 0.5 K for ^{12}CO line emission), MinPts=4, and $\epsilon=1$ are adopted in the DBSCAN algorithm for ^{12}CO clouds identification, as suggested in Yan et al. (2020). In addition, the post-selection criteria are also utilized to avoid noise contamination. For each extracted cloud, it needs to satisfy: (1) the total voxel number is larger than 16; (2) the peak intensity is higher than the ‘cutoff’ adding 3σ ; (3) the angular area is larger than one beam size (2×2 pixels ~ 1 arcmin); and (4) the number of velocity channels is larger than 3. The observational effects, including the finite angular resolution and sensitivity of the observed spectral lines data, on the molecular cloud samples have been systematically investigated in Yan et al. (2022). In addition, the samples extracted by the DBSCAN algorithm also have been compared with those from other algorithms in Yan et al. (2022); Yuan et al. (2022).

^{13}CO structures are defined as a set of contiguous voxels in the PPV space with ^{13}CO line intensities

above a certain threshold, which are extracted using the DBSCAN algorithm within ^{12}CO cloud boundaries. The used DBSCAN parameters are identical to the above parameters for ^{12}CO cloud extraction, except for the post-selection criteria of the peak intensities higher than the ‘cutoff’ adding 2σ , σ is ~ 0.25 K for ^{13}CO line emission. Among the total 18,190 ^{12}CO clouds, 2851 ^{12}CO clouds are identified to have ^{13}CO structures in our paper II. The extracted ^{12}CO line data for 18,190 ^{12}CO clouds and the extracted ^{13}CO structures within the 2851 ^{12}CO clouds are available at DOI:10.57760/sciencedb.j00001.00427 (Yuan et al. 2022a). In this work, we focus on these 2851 ^{12}CO molecular clouds and their internal ^{13}CO structures to investigate the spatial distribution of these internal ^{13}CO structures.

3. RESULTS

3.1. Physical properties of ^{13}CO structures

There are a total of 9566 ^{13}CO structures within the 2851 ^{12}CO molecular clouds. Among that, 1848 ^{13}CO structures (19.3%) are within the ^{12}CO clouds having a single ^{13}CO structure, 886 ^{13}CO structures (9.3%) are from ^{12}CO clouds with double ^{13}CO structures, and 6832 ^{13}CO structures (71.4%) are in the ^{12}CO clouds having more than two ^{13}CO structures (multiple). Based on that, the whole 9,566 ^{13}CO structures are separated into three regimes, i.e. single, double, and multiple.

Figure 1 presents the distributions of physical properties of these ^{13}CO structures in three regimes. The properties include angular areas, velocity spans, peak intensities, and integrated fluxes of the ^{13}CO line emission. Their number distributions for ^{13}CO structures in three regimes are similar, except for that the ‘multiple’ regime exists the ^{13}CO structures having larger values in the angular areas ($\gtrsim 200$ arcmin²), velocity spans ($\gtrsim 10$ km s⁻¹), and integrated fluxes ($\gtrsim 800$ K km s⁻¹ arcmin²). That suggests ^{13}CO gas structures in the ‘multiple’ system can develop into structures having larger spatial scales and higher masses.

Based on the spiral structure model of the Milky Way, ^{12}CO clouds were roughly divided into two groups, i.e. near and far, by a V_{LSR} threshold of -30 km s⁻¹, in the paper I and II. The ^{12}CO clouds in the near group have central velocities ranging from -30 km s⁻¹ to 25 km s⁻¹, and those in the far group are from -95 km s⁻¹ to -30 km s⁻¹. The ^{13}CO structures are also divided into the near or far group, following their natal ^{12}CO clouds. The kinematical distances of these ^{12}CO molecular clouds, estimated using the Bayesian distance calculator in Reid et al. (2016), mainly distribute on \sim

0.5 kpc for clouds in the Local region and ~ 2 kpc for those in the Perseus region. Considering these kinematical distances, the physical scale for the molecular cloud with an angular size of $1'$ in the Local region is ~ 0.15 pc, and the value is ~ 0.6 pc for that in the Perseus region.

Figure 2 presents the number distributions of the angular areas and integrated fluxes of the ^{13}CO structures, which are in the near and far groups, respectively. We find that the angular-area distribution for the observed ^{13}CO structures in the near and far groups is close, as well as the distributions of their integrated fluxes. For the ^{13}CO structures in near group, we fit their power-law distributions as $dN/dX \propto X^{-(\alpha_X+1)}$, the fitted α_A is 0.92 for the angular areas (A) and α_F is 0.73 for the integrated fluxes (F).

In previous works, these localized and discrete subunits in the observed intensity distribution were usually called clumps, such as the clumpy structures traced by the ^{13}CO emission in Blitz & Stark (1986); Williams et al. (1994, 1995); Kramer et al. (1998). These clump masses, which were within various molecular clouds and were identified using different methods (either Gauss-clumps or Clumfind), agree in showing a clump mass spectrum following a power law form $dN/dM \propto M^{-\alpha}$ with a spectral index α between 1.2 and 1.9 (Williams et al. 1994, 1995; Kramer et al. 1998). Assuming the distances for ^{13}CO structures in the same group are close, the mass of a ^{13}CO structure will be proportional to its integrated flux, whose number distribution follows a power law with an exponent of 1.73 ± 0.22 . This value of 1.73 ± 0.22 is in the range of 1.2 – 1.9, thus the results of ^{13}CO structures in Figure 2 are comparable with the previous clump mass spectrum derived in Williams et al. (1994, 1995); Kramer et al. (1998).

3.2. Projected angular separations and radial velocity separations

Since there can be more than one ^{13}CO structure in a single ^{12}CO cloud, how about the relative spatial distribution and kinematical motions between these ^{13}CO structures? We compute the minimal spanning tree (MST) using the Kruskal algorithm in the PYTHON package¹ to connect the whole ^{13}CO structures in a single ^{12}CO cloud together, while minimizing the total sum of the spacings between these ^{13}CO structures. The observed angular separations between ^{13}CO structures are the projection of their true 3-D spacings onto the plane of the sky, which are calculated as the euclidean

¹ <https://docs.scipy.org/doc/scipy/reference/generated/scipy.sparse.csgraph>.

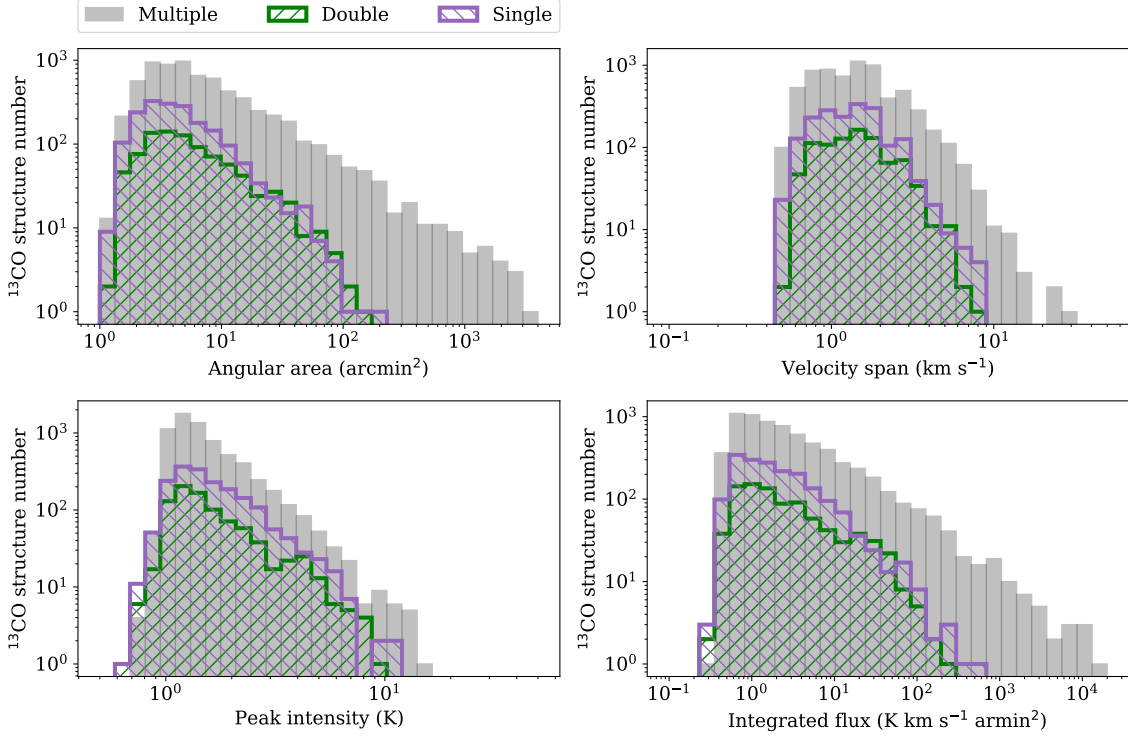


Figure 1. The number distributions of angular area, velocity span, peak intensity, and integrated flux of each individual ^{13}CO structure. The purple, green, and gray histograms represent ^{13}CO structures that are within the ^{12}CO clouds having single, double, and multiple (more than two) ^{13}CO structures, respectively.

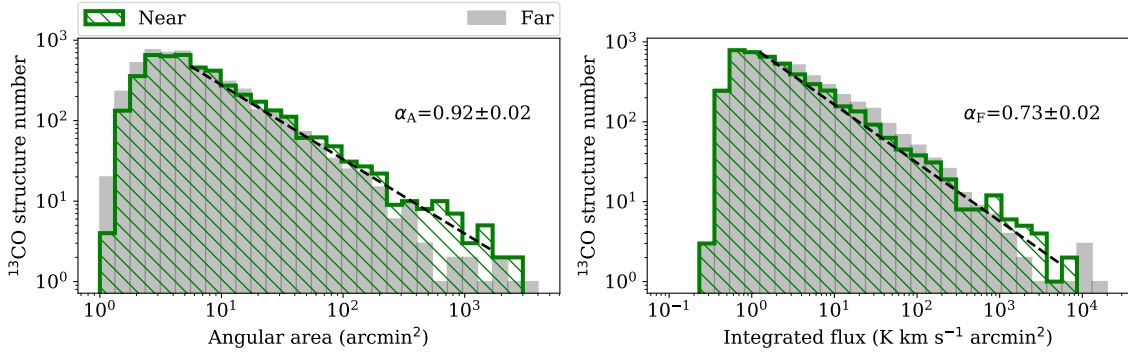


Figure 2. The number distributions of the angular areas (left) and integrated fluxes (right) for ^{13}CO structures in the near and far groups, respectively. The dashed lines fit the power-law distribution, $dN/dX \propto X^{-(\alpha_X+1)}$, for the angular areas and integrated fluxes of ^{13}CO structures in the near group. The fitted α_X is noted in each panel.

distances between the central Galactic coordinates of ^{13}CO structures. Their central Galactic coordinates are the averaged Galactic coordinate over all voxels within extracted ^{13}CO structures, weighted by the corresponding $^{13}\text{CO}(1-0)$ line intensities. The central velocity is the averaged radial velocity over all voxels within the extracted ^{13}CO structure, weighted by the ^{13}CO line intensities (Rosolowsky & Leroy 2006). The radial velocity separations are determined by the absolute differ-

ences between the central velocities of these connected ^{13}CO structures. Figure 3 illustrates the computation of an MST over a ^{12}CO cloud having four ^{13}CO structures. Moreover, we calculate the projected angular separations and the radial velocity separations between ^{13}CO structures along the MST in each ^{12}CO cloud. For the ^{12}CO clouds having double (443) or multiple (560) ^{13}CO structures, the figures showing the distribution of their internal ^{13}CO structures and the computed

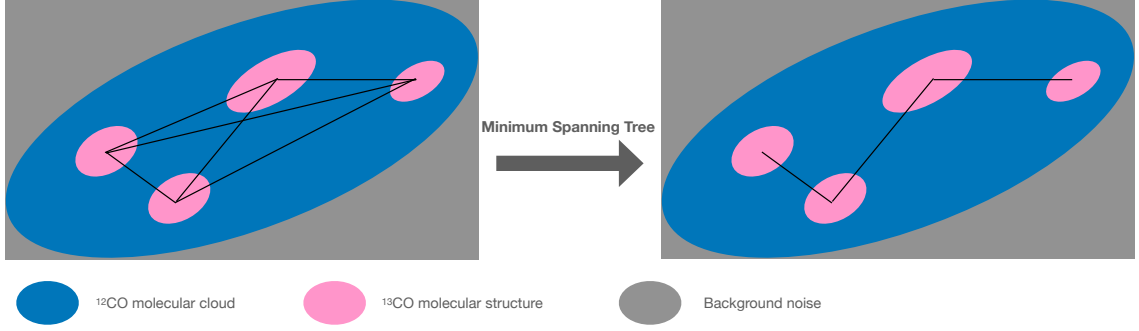


Figure 3. A sketch demonstrating the computation of a minimum spanning tree (MST) over a ^{12}CO cloud having four ^{13}CO structures. **Left panel:** The black lines show the connected graph between each two of the four ^{13}CO structures. **Right panel:** The black lines show an MST, which connects the whole ^{13}CO structures and minimizes the total sum of projected angular separations between ^{13}CO structures.

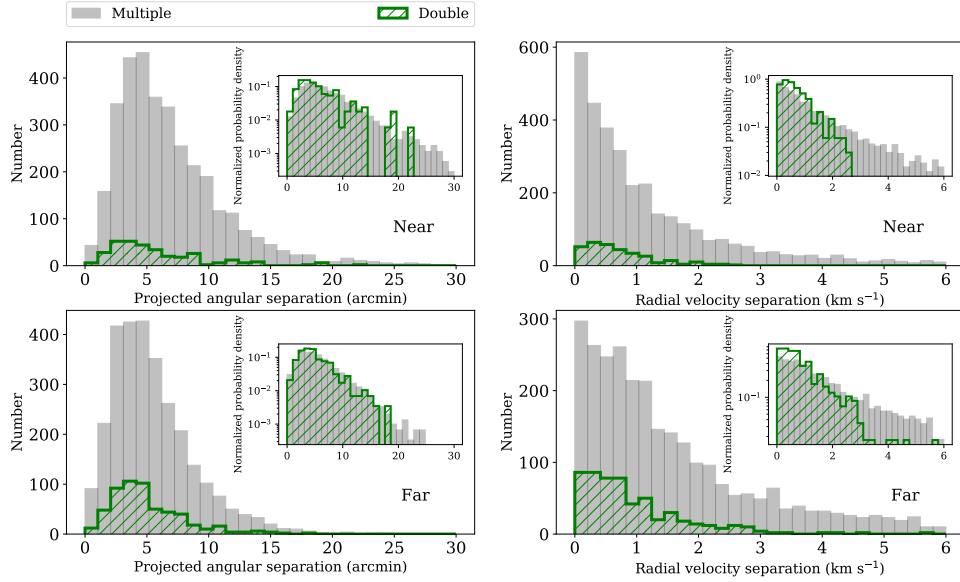


Figure 4. The number distributions of projected angular separations and radial velocity separations between the ^{13}CO structures within ^{12}CO clouds in the near (top) and far (bottom) groups, respectively. The green and gray histograms represent the values from ^{13}CO structures within ^{12}CO clouds having double and multiple ^{13}CO structures, respectively. In the up-right corner of each panel, the histograms present the corresponding distribution of their normalized probability densities. The normalized probability densities are presented as log scales, the separation values are binned as linear scales.

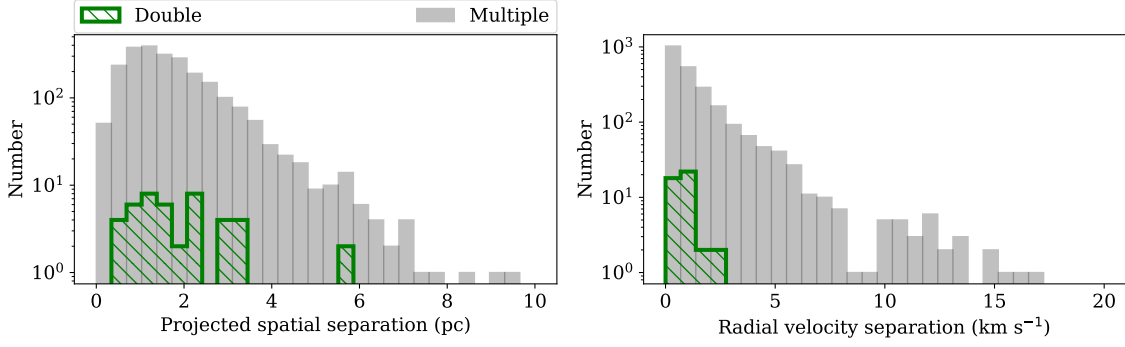


Figure 5. The distributions of the linear separations and radial velocity separations between the ^{13}CO structures within 154 ^{12}CO clouds. These ^{12}CO clouds have available distance information, which are measured with the background-eliminated extinction-parallax method using extinctions and Gaia DR2 parallaxes in Yan et al. (2021a). The green and gray histograms represent the values from ^{13}CO structures within ^{12}CO clouds having double and multiple ^{13}CO structures, respectively. The number of ^{13}CO structures are presented as log scales, the separation values are binned as linear scales.

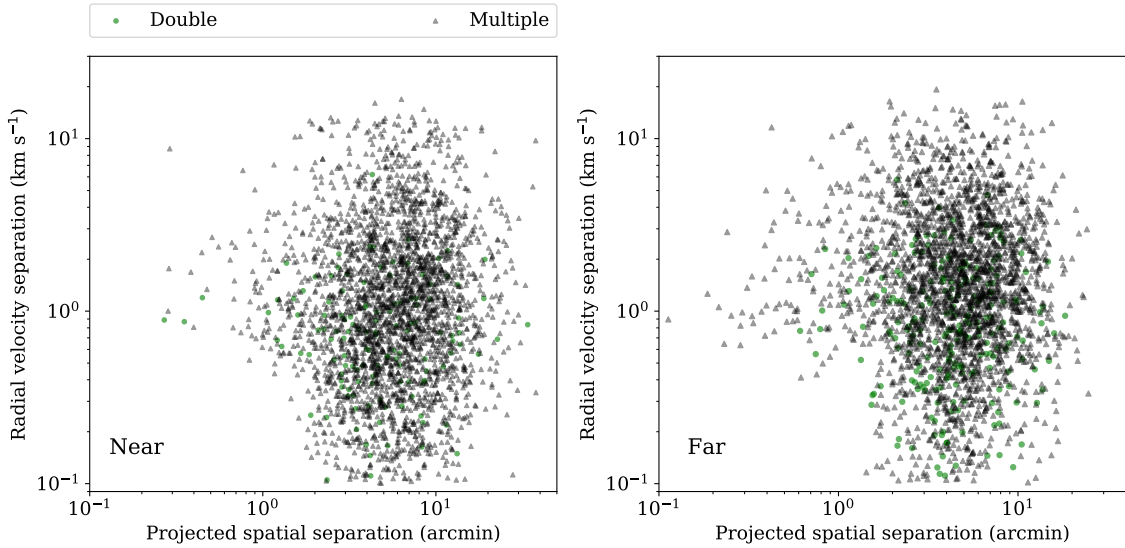


Figure 6. The correlation between the projected angular separations and radial velocity separations of the ^{13}CO structures within ^{12}CO clouds in the near and far groups, respectively. The green and gray points represent the values from ^{13}CO structures in the ‘double’ and ‘multiple’ regime, respectively.

MSTs connecting the ^{13}CO structures are available at DOI:10.57760/sciencedb.06653. In Figure A1 - A8, we present several samples. Moreover, the tables including the values of projected angular separations and radial velocity separations between the ^{13}CO structures with each ^{12}CO cloud are also published in the uniform DOI (Yuan et al. 2022b).

Considering the linear separations of ^{13}CO structures are determined by their angular separations and distances, the resultant separations between ^{13}CO structures are presented as near and far groups. Figure 4

shows the distributions of the projected angular separations and radial velocity separations between the ^{13}CO structures within each ^{12}CO cloud in the near and far groups, respectively. To compare the distribution of separations in the multiple and double regimes, we also plot their normalized probability densities as insets in Figure 4. The normalized probability densities with a large dynamic range of several orders of magnitude are presented as log scales, the corresponding separation values having a narrow range are binned as linear scales. Moreover, the quantiles at 0.05, 0.25, 0.5, 0.75, and 0.95 and the mean values of the projected angular separations and radial velocity separations are also listed in Table 1. For

Table 1. The projected spatial separations and radial velocity separations between ^{13}CO structures within ^{12}CO clouds

Types	Groups	Environment	0.05	0.25	0.5	0.75	0.95	Mean
Spatial separation	Near (arcmin)	Double	1.5	3.0	4.6	7.5	13.6	6.0
		Multiple	2.0	3.8	5.8	8.9	15.3	6.9
	Far (arcmin)	Double	1.5	2.9	4.3	6.6	10.6	5.0
		Multiple	1.4	3.1	4.9	7.1	12.0	5.5
	Subsample (pc)	Double	0.7	1.1	1.6	2.3	3.4	1.9
		Multiple	0.5	1.0	1.5	2.3	3.9	1.8
Velocity separation	Near (km s^{-1})	Double	0.05	0.28	0.57	0.95	1.93	0.75
		Multiple	0.06	0.32	0.8	1.8	5.62	1.52
	Far (km s^{-1})	Double	0.08	0.35	0.71	1.24	2.64	0.94
		Multiple	0.1	0.55	1.2	2.49	6.57	1.98
	Subsample (km s^{-1})	Double	0.11	0.28	0.76	0.95	1.9	0.75
		Multiple	0.06	0.33	0.83	1.77	4.96	1.44

NOTE—The quantiles at 0.05, 0.25, 0.5, 0.75 and 0.95 for each parameter in its sequential data and its mean value. The ‘Near’ and ‘Far’ represent for the MCs in the near and far groups, respectively. The ‘Subsample’ are the 154 MCs with available distance informations. The ‘Double’ and ‘Multiple’ are corresponding to the MCs having double and multiple (more than two) ^{13}CO structures, respectively.

the angular separations, $\sim 50\%$ of the values are in a narrow range of 3 – 7 arcmin. We also find that the ^{13}CO structures in the ‘multiple’ regime have large separations (> 20 arcmin), which are not observed in the ‘double’ regime. Although the angular separations in the far group are slightly lower than those in the near group, the linear separations of ^{13}CO structures in the far group are systematically higher than those in the near group by a factor of ~ 3 , considering the typically kinematical distances of ^{12}CO clouds (~ 0.5 kpc for the near group and ~ 2.0 kpc for the far group). Under the uniform sensitivity and spatial angular resolution, due to the beam dilution effect, the isolated structures with smaller and lower line intensities may be diluted and further undetected, or several small structures are blended together as one structure (Louvet et al. 2021). Hence the observed ^{12}CO clouds and their internal ^{13}CO structures in the far group tend to have relatively large spatial scales and high line intensities. Thus the spatial separations for ^{13}CO structures in the near and far groups may reflect the spatial distribution of ^{13}CO structures with different spatial scales.

For a subsample with 154 ^{12}CO clouds, which have the available distance information from Yan et al. (2021a), the linear separations between their ^{13}CO structures concentrate on a range of 1.0 – 2.3 pc, their median and mean values are about 1.5 pc and 1.8 pc, respec-

tively, as presented in Figure 5. We should note that the MCs in this subsample tend to have large angular sizes, but small distances. $\sim 75\%$ of their distances are less than or close to ~ 1 kpc, mainly in the near group, as presented in Figure B9. Their ^{13}CO structures in the ‘double’ regime are also incomplete. The linear separations from this subsample may not completely represent the distribution of linear separations for the whole ^{13}CO structures, but they still provide a reference for the preferred linear separation in the near group.

For the radial velocity separations between ^{13}CO structures in each ^{12}CO cloud, $\sim 50\%$ of them are in a range of 0.3 – 2.5 km s^{-1} , as listed in Table 1. The ‘multiple’ regime also has large velocity separations ($\sim 3 - 6 \text{ km s}^{-1}$), which are not nearly observed in the ‘double’ regime. In addition, according to their quantiles listed in Table 1, we find the velocity separations in the far group are higher than those in the near group by a factor of ~ 1.3 .

Moreover, in Figure 6, we present the correlation between the projected angular separations and radial velocity separations of ^{13}CO structures in the near and far groups, respectively, the corresponding spearman’s rank correlation coefficients is 0.04 for the near group and - 0.03 for the far group. That suggests there is no obvious correlation between the projected angular separations and radial velocity separations. Both angular

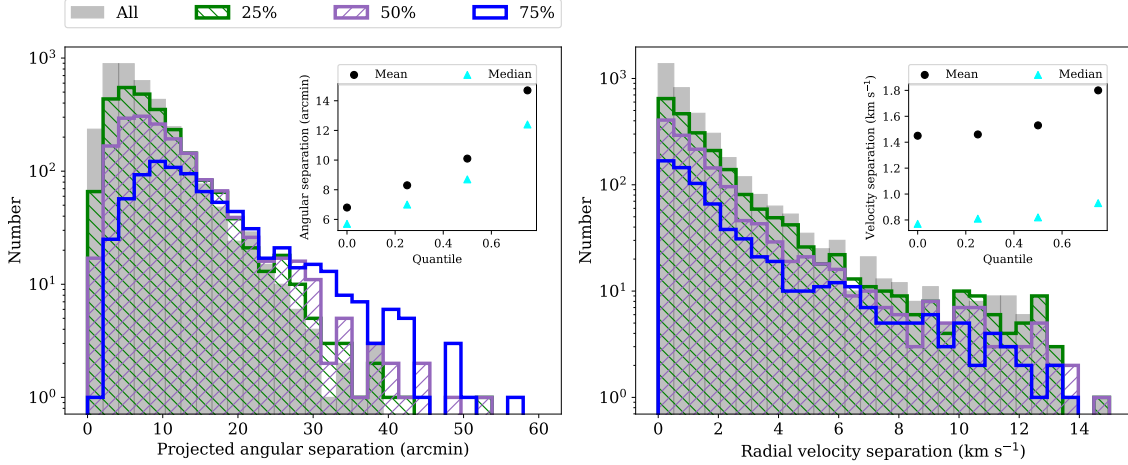


Figure 7. The distribution of angular (left) and velocity (right) separations between the ^{13}CO structures with the different integrated fluxes. The gray histograms represent the whole ^{13}CO structures in the near group. The green, purple, and blue ones represent the near ^{13}CO structures with integrated fluxes larger than their quantile values at 0.25 ($0.9 \text{ K km s}^{-1} \text{ arcmin}^2$), 0.5 ($1.7 \text{ K km s}^{-1} \text{ arcmin}^2$), and 0.75 ($4.6 \text{ K km s}^{-1} \text{ arcmin}^2$), respectively. In the up-right corner of each panel, the scatter plot show the mean (black) and median (cyan) values of angular (left) and velocity (right) separations for each sample.

separations and velocity separations concentrate on a certain range.

Overall, the projected angular separations between ^{13}CO structures, either in the near or far group, center on a range of $\sim 3 - 7 \text{ arcmin}$. Their radial velocity separations mainly distribute from 0.3 km s^{-1} to 2.5 km s^{-1} . The ^{13}CO structures in the ‘multiple’ regime exist large separations, either angular or velocity separations, which are not observed in the ‘double’ regime.

4. DISCUSSION

4.1. Observational effects on the spatial separations of ^{13}CO structures

As mentioned in section 3.2, the linear separations among ^{13}CO structures in the far group are ~ 3 times those of ^{13}CO structures in the near group. Under the uniform sensitivity and spatial angular resolution, the far ^{13}CO structures with relatively small areas and low line intensities may not be observed, or several smaller structures are blended together (Louvét et al. 2021), due to the beam dilution effect. The differences between the linear separations are mainly caused by the observational effects or intrinsic distributions of ^{13}CO structures. This needs a further analysis.

We take the whole ^{13}CO structures in the near group as samples. These near ^{13}CO structures are further grouped into three subsamples, whose ^{13}CO integrated fluxes are larger than the quantile values at 0.25 (subsample-1), 0.5 (subsample-2), and 0.75 (subsample-3) of the ^{13}CO integrated fluxes for the whole samples, respectively. The quantile values at 0.25, 0.5, and 0.75 are 0.9 , 1.7 , and $4.6 \text{ K km s}^{-1} \text{ arcmin}^2$, respectively.

Then we recompute the MST to determine the separations in each subsample. That is, the near ^{13}CO structures with ^{13}CO integrated fluxes less than the $0.9 \text{ K km s}^{-1} \text{ arcmin}^2$ are removed, the rest are taken as the subsample-1 and further used to compute the MST for their parental ^{12}CO clouds. The same process is taken for ^{13}CO structures in subsample-2 and subsample-3.

In figure 7, we present the distributions of the projected angular separations and radial velocity separations for the ^{13}CO structures in the near samples, subsample-1, subsample-2, and subsample-3, respectively. We find that the mean and median angular separations gradually increase from the near sample to the subsamples. While their mean and median values of velocity separations do not vary significantly. The mean and median angular separations for the subsample-3 are about 2 times those in the whole near samples, while the factor is ~ 1.2 for the radial velocity separations.

According to the fitted power-law distribution of $N \propto F^{-0.73}$ for the integrated fluxes in Figure 2, we estimate $l_A \sim 1/\sqrt{N} \sim F^{0.4}$, where l_A is the angular separation. This relation corresponds to the relation between the linear separations and the luminosities ($l_P \sim \mathcal{L}^{0.4}$, where l_P is the linear separation, \mathcal{L} is the luminosity), under the assumption of the close distances for ^{13}CO structures in the near or far group. Thus the linear separations between ^{13}CO structures depend on the number distribution of the observed ^{13}CO structure luminosities. Under the noise rms of 0.25 K and the velocity resolution of 0.17 km s^{-1} for ^{13}CO line data, the integrated fluxes for the extracted ^{13}CO structures by the DBSCAN algorithm are above $\sim 0.5 \text{ K km s}^{-1} \text{ arcmin}^2$. For ^{13}CO

structures in the near and far groups, their kinematical distances concentrate on ~ 0.5 kpc and ~ 2 kpc, respectively. The limited luminosities for the near and far ^{13}CO structures vary by a factor of ~ 16 . According to $l_p \sim \mathcal{L}^{0.4}$, the observed linear separations between ^{13}CO structures in the near group are larger than those in the far group by a factor of 3 ($l_{\text{far}}/l_{\text{near}} \sim \mathcal{L}_{\text{far}}^{0.4}/\mathcal{L}_{\text{near}}^{0.4} \sim 3$), which is consistent with our observed results. Thus we should note that the observed angular separations between ^{13}CO structures depend on the number distribution of their integrated fluxes, which are limited by the spatial resolution and sensitivities of ^{13}CO line data. Considering the observational effects, the whole ^{13}CO structures are separated into near and far groups in the following analysis.

4.2. *Scaling relations between the ^{13}CO structures and their natal ^{12}CO clouds*

After presenting the distributions of the ^{13}CO structure separations within each ^{12}CO cloud, an interesting question concerns whether the relations between the ^{13}CO structure separations and their parental ^{12}CO cloud scales exist.

4.2.1. *A preferred angular separation between ^{13}CO structures within ^{12}CO clouds?*

Figure 8 presents the correlation between the angular areas of the ^{12}CO clouds and the mean angular and velocity separations of ^{13}CO structures. We find that the mean angular separation of ^{13}CO structures in each ^{12}CO cloud is relatively dispersed in the small areas and gradually converge to a constant value (~ 6.9 arcmin for the near group and ~ 5.5 arcmin for the far group) as the increases of ^{12}CO cloud areas. The constant values are the mean value of the whole angular separations in the ‘multiple’ regime, shown as the purple-dashed lines. For the mean velocity separation in each ^{12}CO cloud, there is a similar but slightly ascending trend along with the increase of ^{12}CO cloud areas, their values concentrate in a narrow range of $0.3 - 2.5 \text{ km s}^{-1}$.

Furthermore, we show the correlation between the mean angular separation and the ^{13}CO structure number within each ^{12}CO cloud in Figure 9. There is a similar trend, i.e. the mean angular separation in each ^{12}CO cloud gradually return to a nearly constant value with the increase of the internal ^{13}CO structure number. We also average the mean angular separations in ^{12}CO clouds harboring the same number of ^{13}CO structures. These averaged values are also close to the constant value.

It should be noted that the statistical errors for the mean separations in each ^{12}CO cloud are different, due to that the number of ^{13}CO structures within a single

^{12}CO cloud ranges from 1 to ~ 100 . The mean separations in ^{12}CO clouds with small scales ($\lesssim 10$ ^{13}CO structures) are scattered and those in the ^{12}CO clouds with larger scales ($\gtrsim 10$ ^{13}CO structures) are more centered. Is this trend intrinsic or caused by the statistical errors? To investigate this question, we further present the distributions of the whole angular and velocity separations between ^{13}CO structures in each ^{12}CO cloud, grouped by the number of ^{13}CO structure in their parental ^{12}CO clouds. That is, the separations in the ^{12}CO clouds harboring the same number of ^{13}CO structures are put together, as shown in Figure 10. We find that these projected angular separations distribute in a concentrated range of $\sim 3 - 7$ arcmin, independent of what number of ^{13}CO structures the ^{12}CO clouds have. For each group of separations, which are in the ^{12}CO clouds with the same number of ^{13}CO structures, we also present their mean (purple crosses) and median (cyan squares) values, as well as their standard deviations (purple bars). These mean values are ~ 7 arcmin for the near samples and ~ 5.5 arcmin for the far samples, respectively. Their standard deviations are ~ 4 arcmin for the near samples and ~ 3 arcmin for the far samples.

The radial velocity separations are mainly in a narrow range of $\sim 0.3 - 2.5 \text{ km s}^{-1}$. The mean values for velocity separations in each group are around $\sim 1.2 \text{ km s}^{-1}$ for the near samples and $\sim 1.7 \text{ km s}^{-1}$ for the far samples, also slightly increase to $\sim 2.5 \text{ km s}^{-1}$ in the ^{12}CO clouds having large numbers of ^{13}CO structures ($\gtrsim 80$). In addition, their standard deviations also present a similar trend. One possibility for the increase of the radial velocity separation in the MCs with large scales is the star formation activities within dense structures. As presented in Figure 1, the ^{13}CO structures with large angular areas, velocity spans, and integrated fluxes are observed in the ‘multiple’ regime. Another possibility is due to the projection effect. The MST algorithm used to connect the ^{13}CO structures minimizes the sum of their projected angular separations, not their radial velocity separations. The correspondence between the projected separations in angle and radial separations in velocity for these connected ^{13}CO structures are not straightforward, especially for ^{12}CO clouds having large numbers of ^{13}CO structures.

From above, we find the angular separations between ^{13}CO structures in ^{12}CO clouds, which are in either near or far groups, have nearly uniform mean values and standard deviations. That is, for the MCs at the same distance levels, which span a wide range of angular areas and the harbored ^{13}CO structure counts, the spatial distributions of their internal ^{13}CO structures are nearly consistent. The results also suggest there is

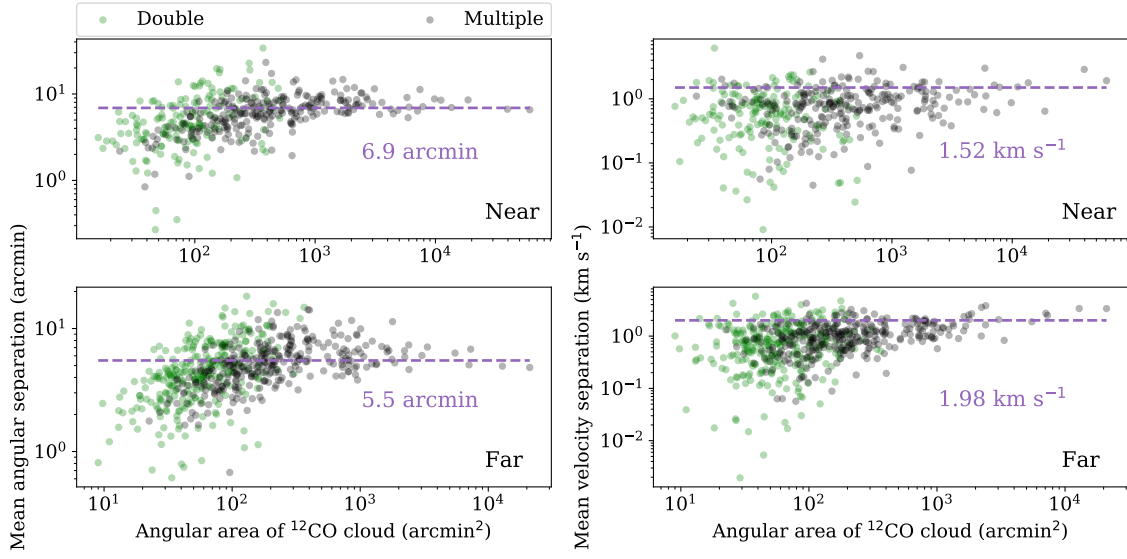


Figure 8. Left panel: the correlations between the mean angular-separation of ^{13}CO structures in each ^{12}CO cloud and the angular area of ^{12}CO cloud in the near and far groups, respectively. Each dot represents a single ^{12}CO cloud, green and gray ones are for the ^{12}CO clouds having double and multiple ^{13}CO structures, respectively. The purple-dashed lines show the mean values for the whole angular separations in the ‘multiple’ regime, which are in the near (6.9 arcmin) and far (5.5 arcmin) groups, respectively. Right panel: the correlations between the mean velocity-separations of ^{13}CO structures in each ^{12}CO cloud and the angular area of ^{12}CO cloud in the near and far groups, respectively. The purple-dashed lines represent the mean values for the whole velocity separations in the ‘multiple’ regime, which are in the near (1.52 km s $^{-1}$) and far (1.98 km s $^{-1}$) groups, respectively.

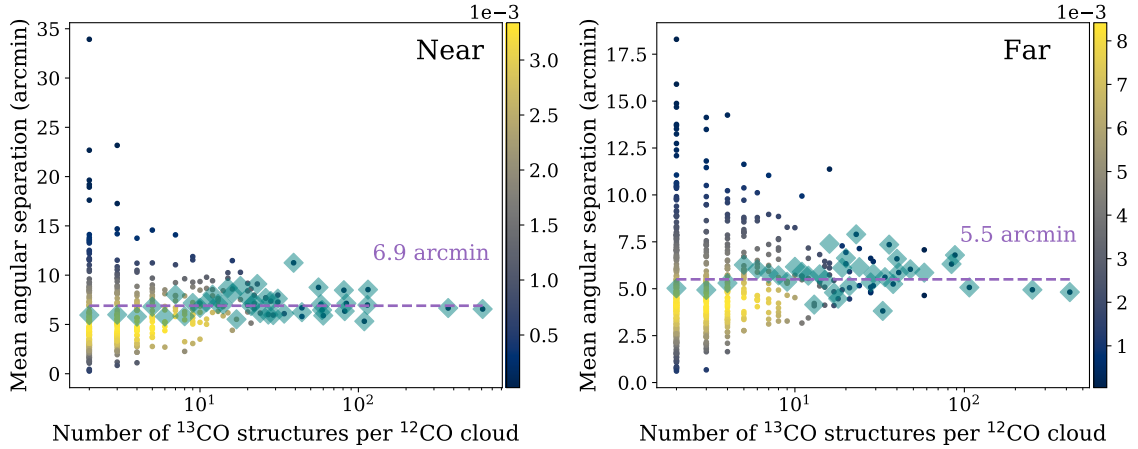


Figure 9. The correlation between the mean angular-separation of ^{13}CO structures within each ^{12}CO cloud and its harbored ^{13}CO structure number in the near and far groups, respectively. Each dot represents a single ^{12}CO cloud. The colors on the dots represent the distribution of the probability density function of the ^{12}CO clouds (2D-PDF), which are calculated utilizing the kernel-density estimation through Gaussian kernels in the PYTHON package [scipy.stats.gaussian_kde](https://docs.scipy.org/doc/scipy/reference/stats.html). The teal diamonds represent the averaged values of the mean angular-separations in the ^{12}CO clouds having a uniform number of ^{13}CO structures. The purple-dashed lines show the mean values for the whole angular separations in the ‘multiple’ regime, which are in the near (6.9 arcmin) and far (5.5 arcmin) groups, respectively.

a preferred angular separation between ^{13}CO structures within these ^{12}CO clouds.

4.2.2. *The development on the internal ^{13}CO structure numbers of ^{12}CO clouds*

Since there is a preferred angular separation between ^{13}CO structures within ^{12}CO clouds, a relation between the spatial scale of ^{12}CO cloud and its harbored ^{13}CO structure number may exist. As presented in Figure 11, we find a trend that the angular area of ^{12}CO cloud increases with its harbored ^{13}CO structures number, although it scatters in the regime for ^{12}CO clouds with several ^{13}CO structures. After taking the median angular areas for the ^{12}CO clouds with the uniform number of ^{13}CO structures, the trend traced by these median values is more obvious. It suggests that the more is their internal ^{13}CO structures, the larger is the angular areas of ^{12}CO clouds, under a preferred angular separation between ^{13}CO structures.

4.2.3. *The development on the maximum ^{13}CO structure in each ^{12}CO cloud*

Since the internal ^{13}CO structure count tend to increase with the ^{12}CO cloud area, how about the area of a single ^{13}CO structure? Do their values change with their parental ^{12}CO cloud's areas? From the distribution of ^{13}CO structure parameters in Figure 1, we find that the ^{13}CO structures in the ‘multiple’ regime have larger values in the angular areas, velocity spans, and integrated fluxes, which are not observed in the ‘single’ and ‘double’ regimes. Here we further investigate the correlation between the maximal angular-area for ^{13}CO structures in each ^{12}CO cloud and the ^{12}CO cloud angular-area.

As presented in Figure 12, there is a roughly positive correlation between the maximal angular-area of ^{13}CO structures in each ^{12}CO cloud and the ^{12}CO cloud angular-area, with the spearman's rank correlation coefficients of 0.7. The teal line shows an upper limit that the whole ^{13}CO emission area in a single ^{12}CO cloud generally do not exceed the 70% of its ^{12}CO emission area (Yuan et al. 2022). The maximal ^{13}CO structures in the ‘double’ and ‘multiple’ systems are lower than the upper limit, but still have a growing tendency among their areas and their parent ^{12}CO cloud areas. Combining the distribution of ^{13}CO structure parameters in the ‘multiple’ regime in Figure 1, we find the ^{12}CO clouds having larger scales tend to have ^{13}CO structures distributed in the larger scales. This result suggests the development of large-scale ^{13}CO structures is synchronized with the spatial scales of ^{12}CO clouds.

4.3. *Implications of molecular clouds assembly and destruction*

Since the spatial distributions of ^{13}CO structures within ^{12}CO molecular clouds spanning a wide range in sizes and environmental conditions are resembled, in addition, there is a preferred angular separation between ^{13}CO structures. These results imply the spatial distribution of internal ^{13}CO structures in molecular clouds are affected by the universal physical mechanism.

The spatial distribution of substructures in molecular clouds, like the dense cores (André et al. 2014; Tafalla & Hacar 2015; Kainulainen et al. 2017; Könyves et al. 2020), young stars (Gomez et al. 1993; Larson 1995; Kraus & Hillenbrand 2008), and young stellar clusters (Grasha et al. 2015) have been investigated. The observed core separations in filaments are interpreted by the two-mode filament fragmentation: for filaments in which the gravitational energy is dominated over turbulent, the “cylindrical” fragmentations occur corresponding to clumps with a separation scale of $\sim 4 \times$ filament width (Inutsuka & Miyama 1992), then the small-scale fragmentations at the effective Jeans length ($\lesssim 0.1$ pc) follow (Clarke et al. 2017; Könyves et al. 2020; Pineda et al. 2022). For young stars, their spatial distributions exhibit self-similar or fractal clustering on the larger scales, and have a clear break from the self-similarity at a small scale, comparable to the Jeans length in typical molecular cloud cores (Larson 1995). Thus, these studies suggest that gravitational instability is responsible for the spacings of small-scale and dense substructures in MCs, like clumps, cores, and young stars. For the MCs with distances information, the observed separations between ^{13}CO structures in MCs are mainly in 1.0 pc – 2.3 pc with a median of 1.5 pc, as listed in Table 1. Under consideration of the densities $n \sim 10^2 - 10^3 \text{ cm}^{-3}$ and $T \sim 10$ K for the MCs, the estimated Jeans length is in the range of ~ 1.4 pc – ~ 0.4 pc. Our observed separations between ^{13}CO structures are systematically larger than the Jeans length scales. This implies the regular separations of ^{13}CO structures within ^{12}CO clouds are hardly interpreted by the Jeans fragmentation.

In another picture, MCs appear to be transient objects that may never reach an equilibrium configuration (Vazquez-Semadeni et al. 1995; Passot et al. 1995; Ballesteros-Paredes et al. 1999b; Vázquez-Semadeni et al. 2003; Clark et al. 2012; Ballesteros-Paredes et al. 2020). They can form in the diffuse ISM through local compressions induced by the converging flows from the differential rotation and shear of the spiral arms (Kwan & Valdes 1983; Tomisaka 1984; Kwan & Valdes 1987), the passage of HII regions or supernova shells (Heiles 1979, 1984; Tenorio-Tagle & Bodenheimer 1988; Hartmann et al. 2001), shock-wave passage (Bergin et al. 2004; Clark et al. 2012; Guo et al. 2021), large-scale

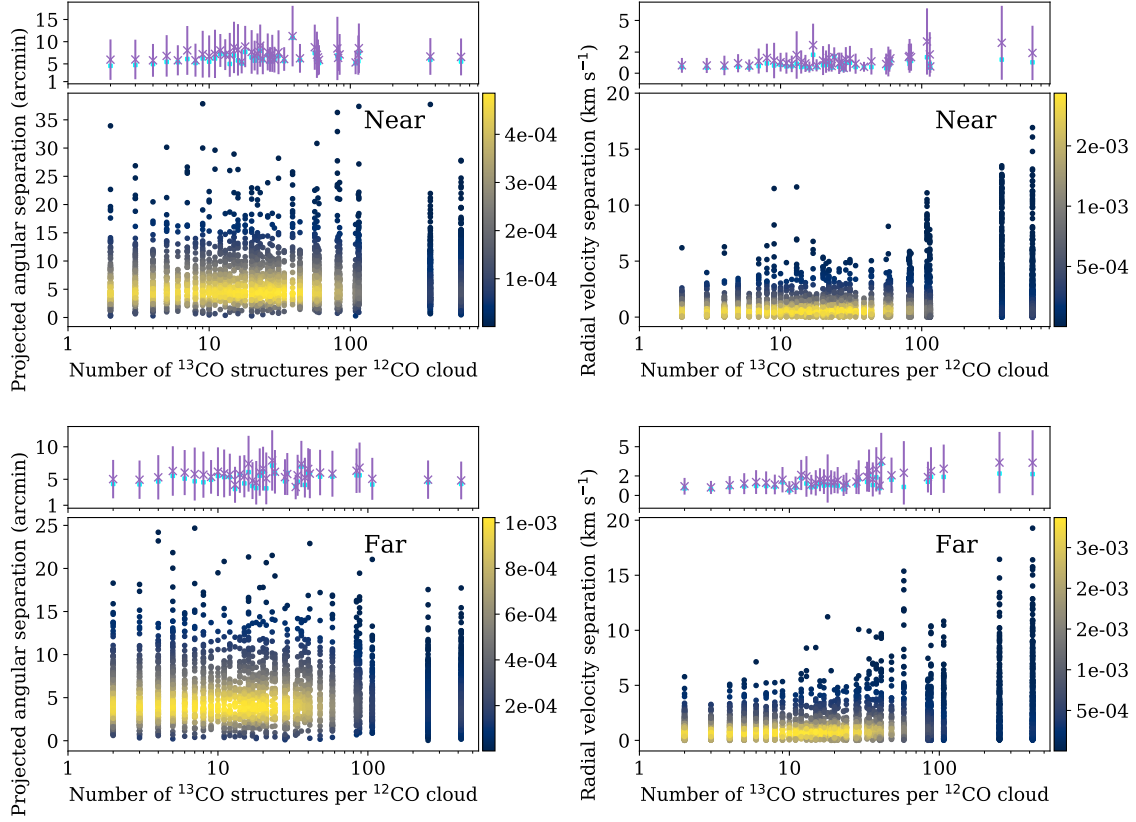


Figure 10. The distribution of the whole projected angular separations and radial velocity separations between ^{13}CO structures within each ^{12}CO cloud in the near and far groups, respectively. These separations are grouped by the ^{13}CO structure number in their natal ^{12}CO clouds. Each dot represents a value for the angular or velocity separation. The colors on the dots represent the distribution of the probability density function of the separation values (2D-PDF). In the top subpanel of each panel, the purple crosses and bars are the mean values and standard variances for the whole separations in ^{12}CO clouds having the same number of ^{13}CO structures. The cyan squares are the median values for those.

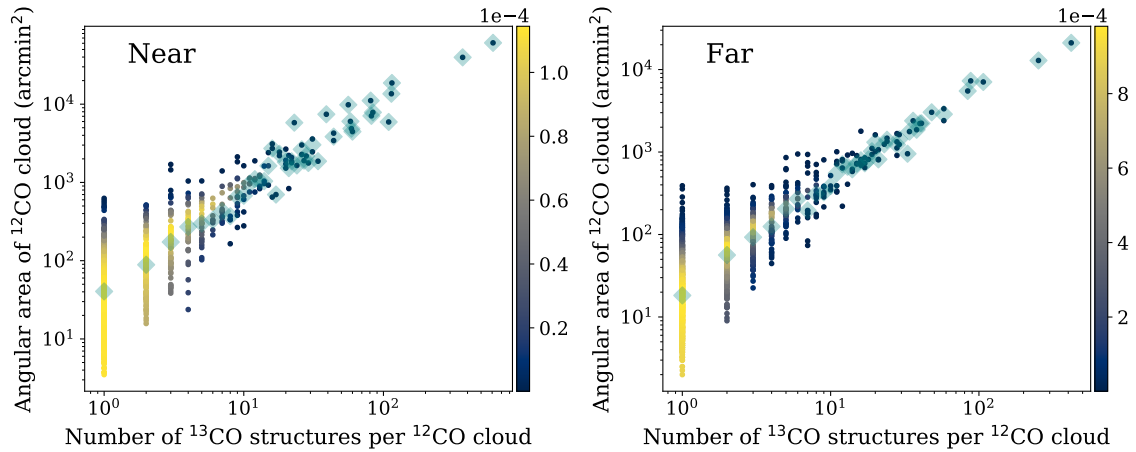


Figure 11. The correlation between the ^{12}CO cloud angular-areas and their harbored ^{13}CO structure number in the near and far groups, respectively. Each dot represents a single ^{12}CO cloud. The colors on the dots represent the distribution of the probability density function of ^{12}CO clouds (2D-PDF). Teal diamonds represent the median values for the angular areas of ^{12}CO clouds having the same number of ^{13}CO structures.

gravitational instability of rotating disk (Lin & Shu 1964; Roberts 1969; Shetty & Ostriker 2008; Tasker & Tan 2009; Dobbs et al. 2011), clouds agglomeration (Oort 1954; Field & Saslaw 1965; Kwan & Valdes 1983; Tomisaka 1984; Dobbs & Baba 2014), and cloud-cloud collisions (Gilden 1984; Fukui et al. 2014, 2016; Dobbs et al. 2015; Gong et al. 2017). In addition, the density fluctuations within MCs can be produced by a common hierarchy of interstellar converging flows, i.e. the supersonic dissipation in the ambient medium (Larson 1981; Myers 1983; Falgarone et al. 1992; Cernicharo et al. 1985; Heyer & Brunt 2004; Falgarone et al. 2009). An evidence generally used to support this picture is the results of the probability density functions of the molecular hydrogen column density (N-PDFs) of MCs (Vazquez-Semadeni 1994; Padoan et al. 1997; Scalo et al. 1998; Klessen et al. 2000). Ma et al. (2021, 2022) has analyzed the N-PDFs for a sample of MCs using ^{13}CO lines, and found that $\sim 72\%$ of them present a log-normal distribution and 18% are fitted by a log-normal plus power-law function. However, none of the transient models provide the prediction for the regular separations between ^{13}CO structures within ^{12}CO clouds so far. Our observed results will provide a constraint for the transient picture of MCs. Most likely, the preferred separation will provide a fundamental unit for the assembly and destruction of MCs.

From the scaling relations between the ^{12}CO clouds and their internal ^{13}CO structures, the spatial scales of ^{12}CO clouds increase with their harbored ^{13}CO structures number, under a preferred angular separation between ^{13}CO structures. Among our 2851 MC samples, $\sim 60\%$ harbor one single ^{13}CO structure, $\sim 15\%$ have double ^{13}CO structures, the rest $\sim 20\%$ have multiple (more than two) ^{13}CO structures, as presented in Figure 11 in Yuan et al. (2022). The mean and spread of the angular separations between ^{13}CO structures within these ^{12}CO clouds are resembled, independent of the ^{12}CO cloud scales. According to these results, we propose an alternative picture for the assembly and destruction of molecular clouds: there is a fundamental separation between the internal structures of molecular clouds, hence the build-up or destruction of molecular clouds proceeds under this fundamental unit, although the origin of this fundamental separation is still needed to be identified. Moreover, the ^{12}CO clouds having larger scales tend to have ^{13}CO structures with larger scales, as mentioned in Section 4.2.3. That suggests the development of large-scale ^{13}CO structures is synchronized with the ^{12}CO cloud scales. Follow-up analysis on the velocity structures of MCs is essential for us to further verify this picture. The transient configuration and fundamental

separations between high-density substructures can regulate the mass agglomeration in MCs, and further prevent higher star formation efficiency. Therefore the picture of fundamental units provides a natural explanation for the low star formation rate in MCs.

5. CONCLUSIONS

We use a sample of 2851 ^{12}CO molecular clouds, inside which a total of 9566 ^{13}CO gas structures are identified, to systematically investigate the spatial distribution and relative motion of ^{13}CO structures within ^{12}CO molecular clouds. The main conclusions are as follows:

1. The projected angular separations center on a range of $\sim 3 - 7$ arcmin with a median of ~ 5 arcmin, and the radial velocity separations mainly distribute from $\sim 0.3 \text{ km s}^{-1}$ to 2.5 km s^{-1} . The observed angular separations depend on the integrated fluxes spectra of the observed ^{13}CO structures, which is limited by the spatial resolution and sensitivities of ^{13}CO line data.
2. The angular separations between ^{13}CO structures within ^{12}CO clouds have a preferred value, independent of the ^{12}CO cloud angular areas and the numbers of their internal ^{13}CO structure.
3. A scaling relation showing the ^{12}CO cloud area increases with its internal ^{13}CO structure count is revealed. Moreover, it is found that the maximum angular area of ^{13}CO structures in each ^{12}CO cloud tends to increase with the angular area of ^{12}CO cloud itself.

This research made use of the data from the Milky Way Imaging Scroll Painting (MWISP) project, which is a multi-line survey in $^{12}\text{CO}/^{13}\text{CO}/\text{C}^{18}\text{O}$ along the northern galactic plane with PMO-13.7m telescope. We are grateful to all of the members of the MWISP working group, particularly to the staff members at the PMO-13.7m telescope, for their long-term support. This work was supported by the National Natural Science Foundation of China through grant 12041305. F. Du is also supported by NNSFC through grant 11873094. MWISP was sponsored by the National Key R&D Program of China with grant 2017YFA0402701 and the CAS Key Research Program of Frontier Sciences with grant QYZDJ-SSW-SLH047.

Software: Astropy (Astropy Collaboration et al. 2013, 2018), Scipy (Virtanen et al. 2020), Matplotlib (Hunter 2007)

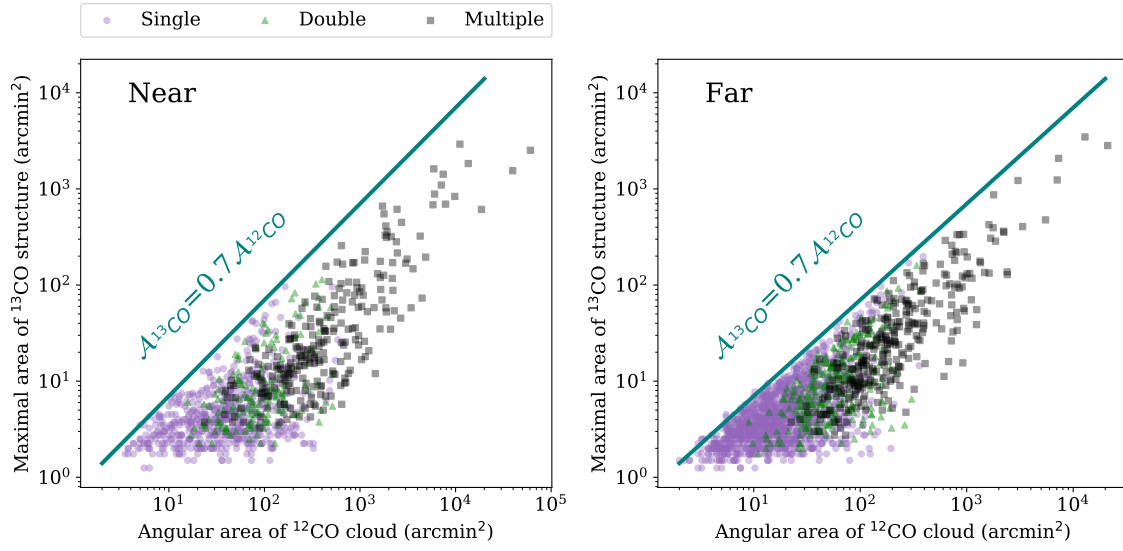


Figure 12. The correlation between the maximum angular-area of ^{13}CO structures within a single ^{12}CO cloud and the angular area of its natal ^{12}CO cloud. Each dot represents a single ^{12}CO cloud, purple, green and gray ones are for the ^{12}CO clouds having single, double and multiple ^{13}CO structures, respectively. The teal lines show an upper limit that the whole ^{13}CO emission area in a single MC generally do not exceed the 70% of its ^{12}CO emission area (Yuan et al. 2022).

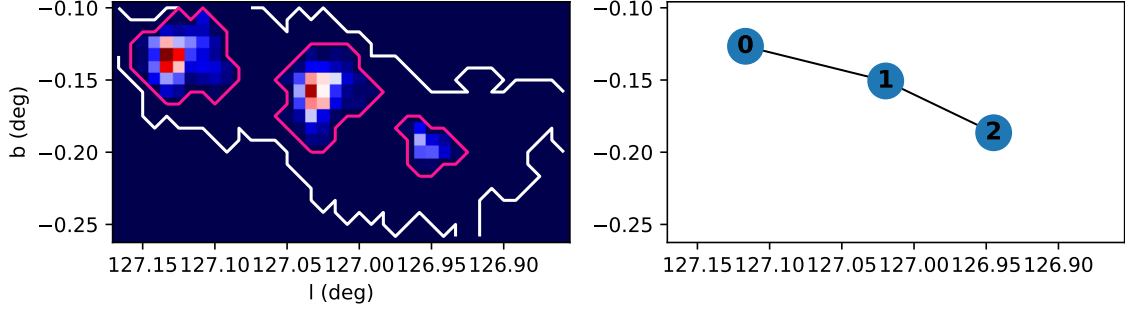


Figure A1. Left panel: the colormap represents the distribution of the velocity-integrated intensities of ^{13}CO line emission within a ^{12}CO cloud. The white and magenta contours indicate the boundaries of the ^{12}CO cloud and ^{13}CO structures, which are identified by the DBSCAN algorithm. Right panel: the minimal spanning tree connects the internal ^{13}CO structures over a ^{12}CO cloud. Each node sites the central Galactic coordinates for a ^{13}CO structure.

APPENDIX

A. EXAMPLES ON THE MINIMAL SPANNING TREE OVER ^{12}CO CLOUDS

Figure A1 - A8 present the ^{13}CO structures within several ^{12}CO molecular clouds and the calculated MSTs connecting the ^{13}CO structures.

B. THE DISTANCES FOR 154 MOLECULAR CLOUDS

Figure B9 presents the distribution of the distances for 154 molecular clouds. Their distances are measured with the extinctions and Gaia DR2 parallaxes through the background-eliminated extinction-parallax method in (Yan et al. 2021a).

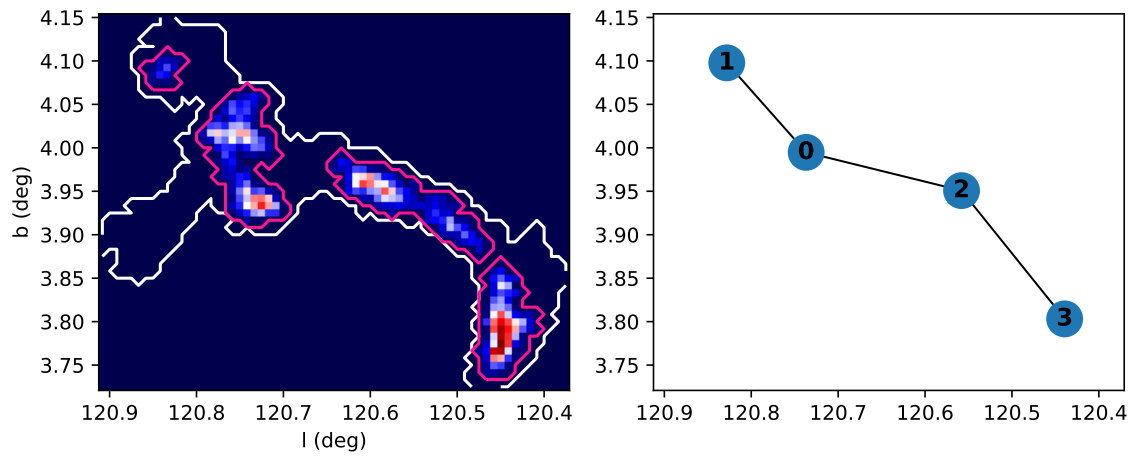


Figure A2. Continued from Fig. A1.

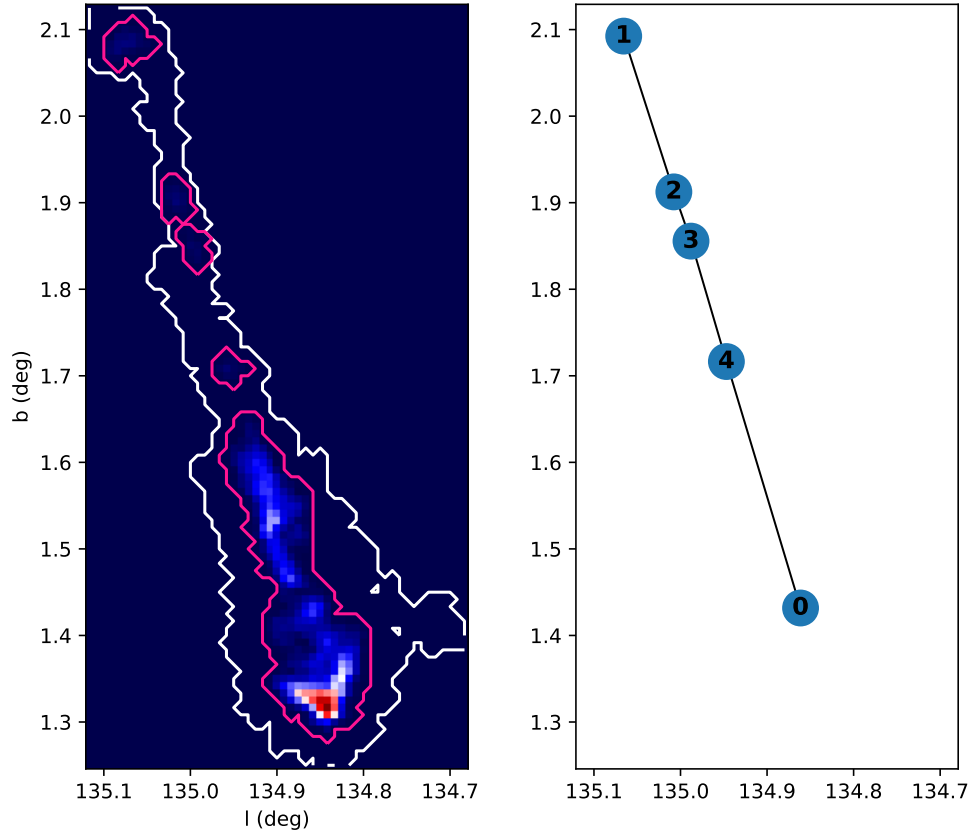


Figure A3. Continued from Fig. A1.

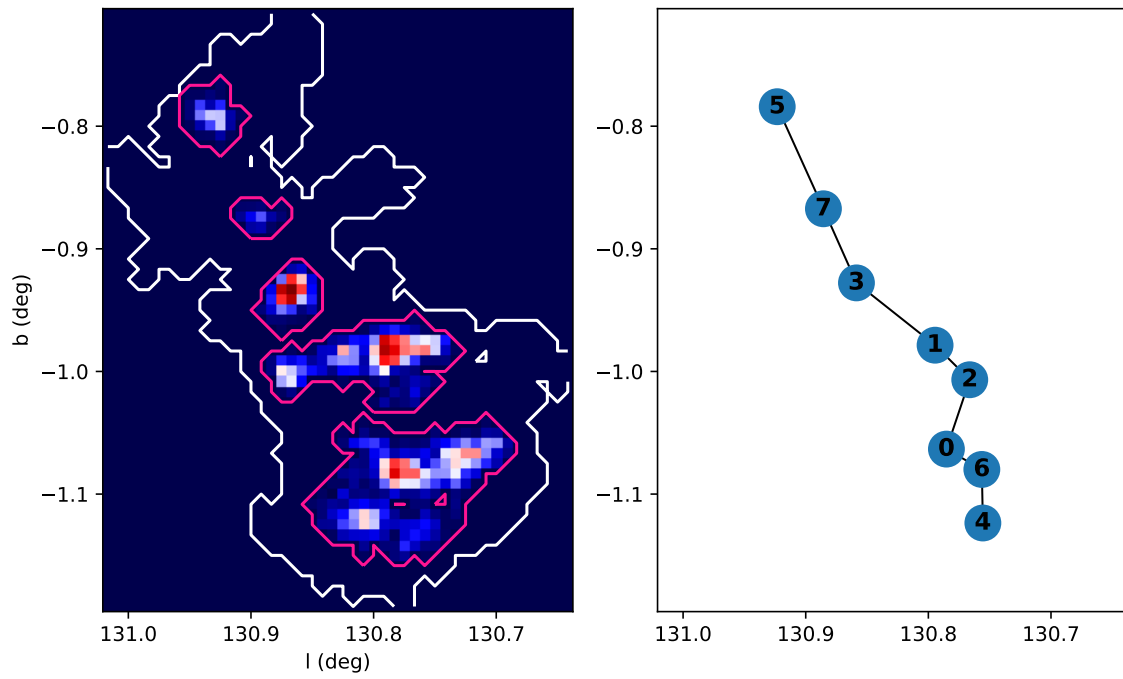


Figure A4. Continued from Fig. A1.

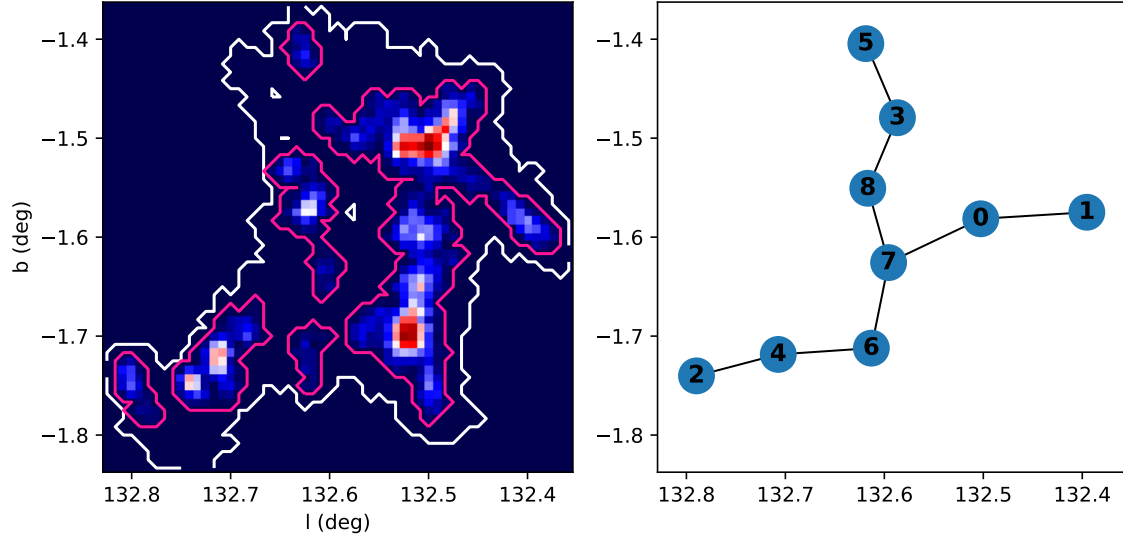


Figure A5. Continued from Fig. A1.

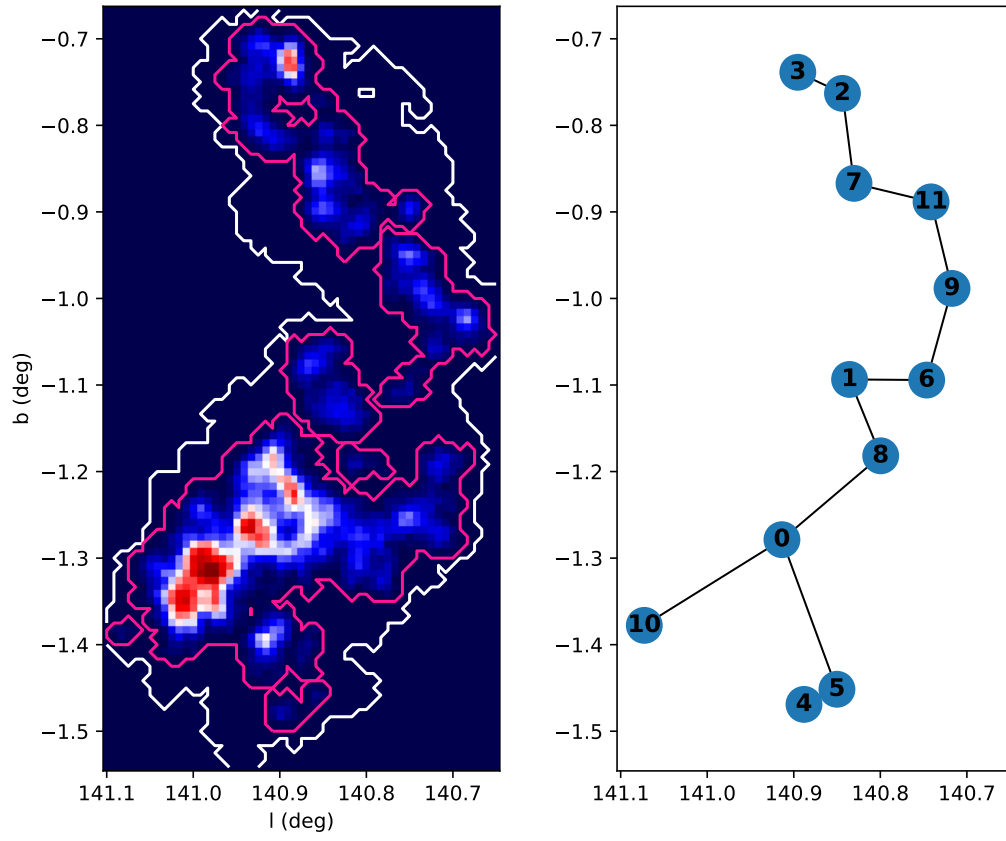


Figure A6. Continued from Fig. A1.

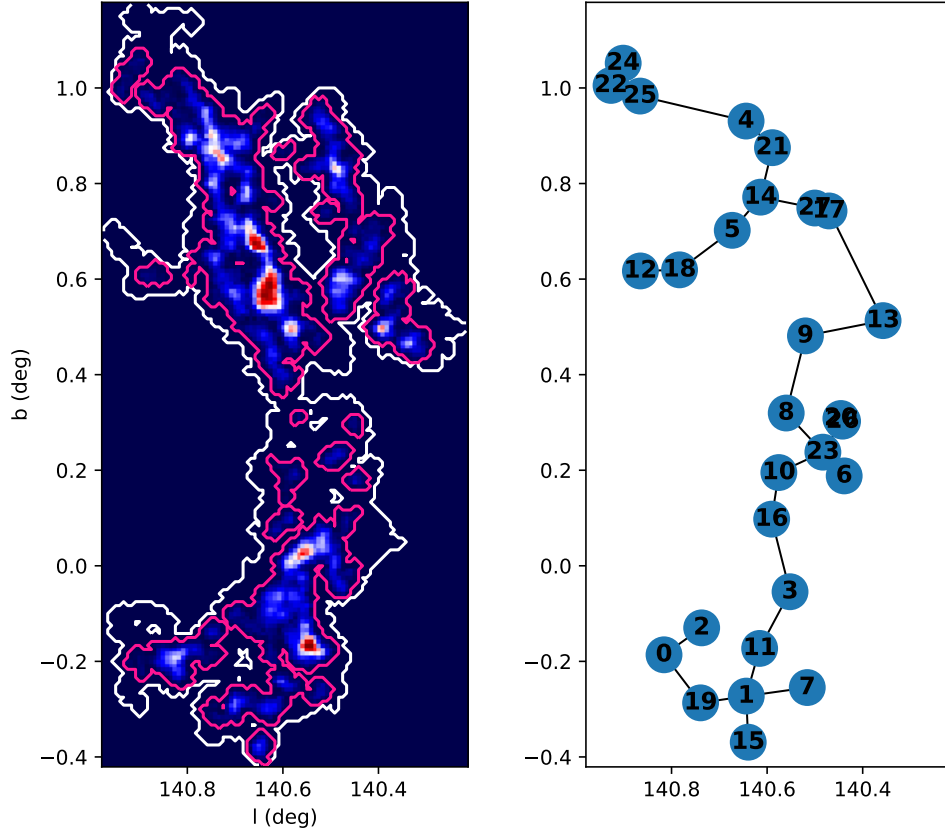


Figure A7. Continued from Fig. A1.

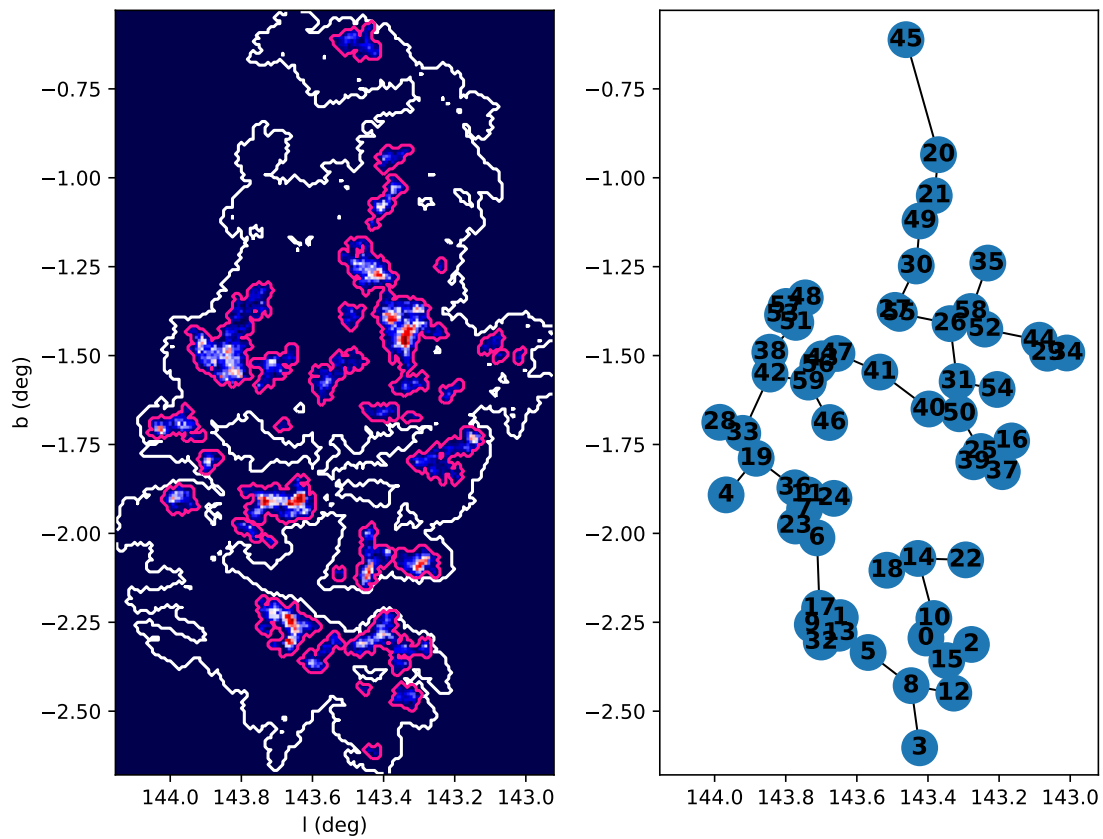


Figure A8. Continued from Fig. A1.

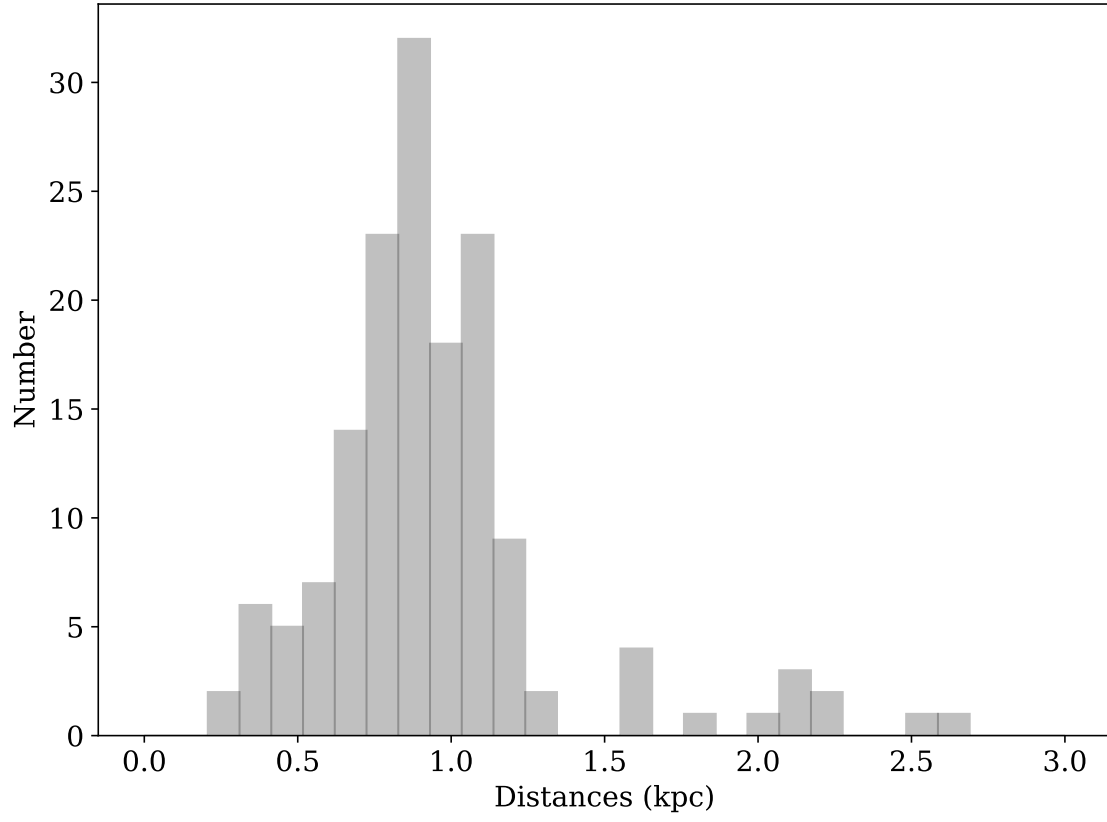


Figure B9. The distribution of the distances for the subsamples from [Yan et al. \(2020\)](#).

REFERENCES

- André, P., Di Francesco, J., Ward-Thompson, D., et al. 2014, in *Protostars and Planets VI*, ed. H. Beuther, R. S. Klessen, C. P. Dullemond, & T. Henning, 27, doi: [10.2458/azu_uapress.9780816531240-ch002](https://doi.org/10.2458/azu_uapress.9780816531240-ch002)
- André, P., Men'shchikov, A., Bontemps, S., et al. 2010, *A&A*, 518, L102, doi: [10.1051/0004-6361/201014666](https://doi.org/10.1051/0004-6361/201014666)
- André, P., Revéret, V., Könyves, V., et al. 2016, *A&A*, 592, A54, doi: [10.1051/0004-6361/201628378](https://doi.org/10.1051/0004-6361/201628378)
- Arzoumanian, D., André, P., Didelon, P., et al. 2011, *A&A*, 529, L6, doi: [10.1051/0004-6361/201116596](https://doi.org/10.1051/0004-6361/201116596)
- Astropy Collaboration, Robitaille, T. P., Tollerud, E. J., et al. 2013, *A&A*, 558, A33, doi: [10.1051/0004-6361/201322068](https://doi.org/10.1051/0004-6361/201322068)
- Astropy Collaboration, Price-Whelan, A. M., Sipőcz, B. M., et al. 2018, *AJ*, 156, 123, doi: [10.3847/1538-3881/aabc4f](https://doi.org/10.3847/1538-3881/aabc4f)
- Ballesteros-Paredes, J., Vázquez-Semadeni, E., & Scalo, J. 1999a, *ApJ*, 515, 286, doi: [10.1086/307007](https://doi.org/10.1086/307007)
- . 1999b, *ApJ*, 515, 286, doi: [10.1086/307007](https://doi.org/10.1086/307007)
- Ballesteros-Paredes, J., André, P., Hennebelle, P., et al. 2020, *SSRv*, 216, 76, doi: [10.1007/s11214-020-00698-3](https://doi.org/10.1007/s11214-020-00698-3)
- Bergin, E. A., Hartmann, L. W., Raymond, J. C., & Ballesteros-Paredes, J. 2004, *ApJ*, 612, 921, doi: [10.1086/422578](https://doi.org/10.1086/422578)
- Beuther, H., Wang, Y., Soler, J., et al. 2020, *A&A*, 638, A44, doi: [10.1051/0004-6361/202037950](https://doi.org/10.1051/0004-6361/202037950)
- Blitz, L., & Stark, A. A. 1986, *ApJL*, 300, L89, doi: [10.1086/184609](https://doi.org/10.1086/184609)
- Cernicharo, J., Bachiller, R., & Duvert, G. 1985, *A&A*, 149, 273
- Clark, P. C., Glover, S. C. O., Klessen, R. S., & Bonnell, I. A. 2012, *MNRAS*, 424, 2599, doi: [10.1111/j.1365-2966.2012.21259.x](https://doi.org/10.1111/j.1365-2966.2012.21259.x)
- Clarke, S. D., Whitworth, A. P., Duarte-Cabral, A., & Hubber, D. A. 2017, *MNRAS*, 468, 2489, doi: [10.1093/mnras/stx637](https://doi.org/10.1093/mnras/stx637)
- Dobbs, C., & Baba, J. 2014, *PASA*, 31, e035, doi: [10.1017/pasa.2014.31](https://doi.org/10.1017/pasa.2014.31)
- Dobbs, C. L., Burkert, A., & Pringle, J. E. 2011, *MNRAS*, 417, 1318, doi: [10.1111/j.1365-2966.2011.19346.x](https://doi.org/10.1111/j.1365-2966.2011.19346.x)
- Dobbs, C. L., Pringle, J. E., & Duarte-Cabral, A. 2015, *MNRAS*, 446, 3608, doi: [10.1093/mnras/stu2319](https://doi.org/10.1093/mnras/stu2319)
- Ester, M., Kriegel, H.-P., Sander, J., & Xu, X. 1996, in *Proceedings of the Second International Conference on Knowledge Discovery and Data Mining, KDD'96 (AAAI Press)*, 226–231. <http://dl.acm.org/citation.cfm?id=3001460.3001507>
- Falgarone, E., Pety, J., & Hily-Blant, P. 2009, *A&A*, 507, 355, doi: [10.1051/0004-6361/200810963](https://doi.org/10.1051/0004-6361/200810963)
- Falgarone, E., Puget, J. L., & Perault, M. 1992, *A&A*, 257, 715
- Field, G. B., & Saslaw, W. C. 1965, *ApJ*, 142, 568, doi: [10.1086/148318](https://doi.org/10.1086/148318)
- Fukui, Y., Ohama, A., Hanaoka, N., et al. 2014, *ApJ*, 780, 36, doi: [10.1088/0004-637X/780/1/36](https://doi.org/10.1088/0004-637X/780/1/36)
- Fukui, Y., Torii, K., Ohama, A., et al. 2016, *ApJ*, 820, 26, doi: [10.3847/0004-637X/820/1/26](https://doi.org/10.3847/0004-637X/820/1/26)
- Gilden, D. L. 1984, *ApJ*, 279, 335, doi: [10.1086/161894](https://doi.org/10.1086/161894)
- Goldreich, P., & Lynden-Bell, D. 1965, *MNRAS*, 130, 97, doi: [10.1093/mnras/130.2.97](https://doi.org/10.1093/mnras/130.2.97)
- Gomez, M., Hartmann, L., Kenyon, S. J., & Hewett, R. 1993, *AJ*, 105, 1927, doi: [10.1086/116567](https://doi.org/10.1086/116567)
- Gong, Y., Fang, M., Mao, R., et al. 2017, *ApJL*, 835, L14, doi: [10.3847/2041-8213/835/1/L14](https://doi.org/10.3847/2041-8213/835/1/L14)
- Grasha, K., Calzetti, D., Adamo, A., et al. 2015, *ApJ*, 815, 93, doi: [10.1088/0004-637X/815/2/93](https://doi.org/10.1088/0004-637X/815/2/93)
- Guo, W., Chen, X., Feng, J., et al. 2021, *ApJ*, 921, 23, doi: [10.3847/1538-4357/ac15fe](https://doi.org/10.3847/1538-4357/ac15fe)
- Hacar, A., Clark, S., Heitsch, F., et al. 2022, arXiv e-prints, arXiv:2203.09562. <https://arxiv.org/abs/2203.09562>
- Hacar, A., Tafalla, M., Forbrich, J., et al. 2018, *A&A*, 610, A77, doi: [10.1051/0004-6361/201731894](https://doi.org/10.1051/0004-6361/201731894)
- Hacar, A., Tafalla, M., Kauffmann, J., & Kovács, A. 2013, *A&A*, 554, A55, doi: [10.1051/0004-6361/201220090](https://doi.org/10.1051/0004-6361/201220090)
- Hartmann, L., Ballesteros-Paredes, J., & Bergin, E. A. 2001, *ApJ*, 562, 852, doi: [10.1086/323863](https://doi.org/10.1086/323863)
- Heiles, C. 1979, *ApJ*, 229, 533, doi: [10.1086/156986](https://doi.org/10.1086/156986)
- . 1984, *ApJS*, 55, 585, doi: [10.1086/190970](https://doi.org/10.1086/190970)
- Heitsch, F., Slyz, A. D., Devriendt, J. E. G., Hartmann, L. W., & Burkert, A. 2006, *ApJ*, 648, 1052, doi: [10.1086/505931](https://doi.org/10.1086/505931)
- Heyer, M. H., & Brunt, C. M. 2004, *ApJL*, 615, L45, doi: [10.1086/425978](https://doi.org/10.1086/425978)
- Hunter, J. D. 2007, *Computing in Science & Engineering*, 9, 90, doi: [10.1109/MCSE.2007.55](https://doi.org/10.1109/MCSE.2007.55)
- Inutsuka, S.-I., & Miyama, S. M. 1992, *ApJ*, 388, 392, doi: [10.1086/171162](https://doi.org/10.1086/171162)
- Kainulainen, J., Stutz, A. M., Stanke, T., et al. 2017, *A&A*, 600, A141, doi: [10.1051/0004-6361/201628481](https://doi.org/10.1051/0004-6361/201628481)
- Klessen, R. S., Heitsch, F., & Mac Low, M.-M. 2000, *ApJ*, 535, 887, doi: [10.1086/308891](https://doi.org/10.1086/308891)
- Könyves, V., André, P., Men'shchikov, A., et al. 2015, *A&A*, 584, A91, doi: [10.1051/0004-6361/201525861](https://doi.org/10.1051/0004-6361/201525861)
- Könyves, V., André, P., Arzoumanian, D., et al. 2020, *A&A*, 635, A34, doi: [10.1051/0004-6361/201834753](https://doi.org/10.1051/0004-6361/201834753)
- Kramer, C., Stutzki, J., Rohrig, R., & Corneliussen, U. 1998, *A&A*, 329, 249

- Kraus, A. L., & Hillenbrand, L. A. 2008, *ApJL*, 686, L111, doi: [10.1086/593012](https://doi.org/10.1086/593012)
- Kwan, J., & Valdes, F. 1983, *ApJ*, 271, 604, doi: [10.1086/161227](https://doi.org/10.1086/161227)
- . 1987, *ApJ*, 315, 92, doi: [10.1086/165116](https://doi.org/10.1086/165116)
- Larson, R. B. 1981, *MNRAS*, 194, 809, doi: [10.1093/mnras/194.4.809](https://doi.org/10.1093/mnras/194.4.809)
- . 1995, *MNRAS*, 272, 213, doi: [10.1093/mnras/272.1.213](https://doi.org/10.1093/mnras/272.1.213)
- Li, G.-X., Wyrowski, F., Menten, K., & Belloche, A. 2013, *A&A*, 559, A34, doi: [10.1051/0004-6361/201322411](https://doi.org/10.1051/0004-6361/201322411)
- Lin, C. C., & Shu, F. H. 1964, *ApJ*, 140, 646, doi: [10.1086/147955](https://doi.org/10.1086/147955)
- Louvet, F., Hennebelle, P., Men'shchikov, A., et al. 2021, *A&A*, 653, A157, doi: [10.1051/0004-6361/202040053](https://doi.org/10.1051/0004-6361/202040053)
- Ma, Y., Wang, H., Li, C., et al. 2021, *ApJS*, 254, 3, doi: [10.3847/1538-4365/abe85c](https://doi.org/10.3847/1538-4365/abe85c)
- Ma, Y., Wang, H., Zhang, M., et al. 2022, *ApJS*, 262, 16, doi: [10.3847/1538-4365/ac7797](https://doi.org/10.3847/1538-4365/ac7797)
- Mattern, M., Kauffmann, J., Csengeri, T., et al. 2018, *A&A*, 619, A166, doi: [10.1051/0004-6361/201833406](https://doi.org/10.1051/0004-6361/201833406)
- Molinari, S., Swinyard, B., Bally, J., et al. 2010, *A&A*, 518, L100, doi: [10.1051/0004-6361/201014659](https://doi.org/10.1051/0004-6361/201014659)
- Myers, P. C. 1983, *ApJ*, 270, 105, doi: [10.1086/161101](https://doi.org/10.1086/161101)
- . 2009, *ApJ*, 700, 1609, doi: [10.1088/0004-637X/700/2/1609](https://doi.org/10.1088/0004-637X/700/2/1609)
- Oort, J. H. 1954, *BAN*, 12, 177
- Padoan, P., Nordlund, A., & Jones, B. J. T. 1997, *MNRAS*, 288, 145, doi: [10.1093/mnras/288.1.145](https://doi.org/10.1093/mnras/288.1.145)
- Passot, T., Vázquez-Semadeni, E., & Pouquet, A. 1995, *ApJ*, 455, 536, doi: [10.1086/176603](https://doi.org/10.1086/176603)
- Pineda, J. E., Arzoumanian, D., André, P., et al. 2022, *arXiv e-prints*, arXiv:2205.03935, <https://arxiv.org/abs/2205.03935>
- Polychroni, D., Schisano, E., Elia, D., et al. 2013, *ApJL*, 777, L33, doi: [10.1088/2041-8205/777/2/L33](https://doi.org/10.1088/2041-8205/777/2/L33)
- Reid, M. J., Dame, T. M., Menten, K. M., & Brunthaler, A. 2016, *ApJ*, 823, 77, doi: [10.3847/0004-637X/823/2/77](https://doi.org/10.3847/0004-637X/823/2/77)
- Roberts, W. W. 1969, *ApJ*, 158, 123, doi: [10.1086/150177](https://doi.org/10.1086/150177)
- Rosolowsky, E., & Leroy, A. 2006, *PASP*, 118, 590, doi: [10.1086/502982](https://doi.org/10.1086/502982)
- Scalo, J., Vázquez-Semadeni, E., Chappell, D., & Passot, T. 1998, *ApJ*, 504, 835, doi: [10.1086/306099](https://doi.org/10.1086/306099)
- Schisano, E., Rygl, K. L. J., Molinari, S., et al. 2014, *ApJ*, 791, 27, doi: [10.1088/0004-637X/791/1/27](https://doi.org/10.1088/0004-637X/791/1/27)
- Shetty, R., & Ostriker, E. C. 2008, *ApJ*, 684, 978, doi: [10.1086/590383](https://doi.org/10.1086/590383)
- Su, Y., Yang, J., Zhang, S., et al. 2019, *ApJS*, 240, 9, doi: [10.3847/1538-4365/aaf1c8](https://doi.org/10.3847/1538-4365/aaf1c8)
- Tafalla, M., & Hacar, A. 2015, *A&A*, 574, A104, doi: [10.1051/0004-6361/201424576](https://doi.org/10.1051/0004-6361/201424576)
- Tasker, E. J., & Tan, J. C. 2009, *ApJ*, 700, 358, doi: [10.1088/0004-637X/700/1/358](https://doi.org/10.1088/0004-637X/700/1/358)
- Tenorio-Tagle, G., & Bodenheimer, P. 1988, *ARA&A*, 26, 145, doi: [10.1146/annurev.aa.26.090188.001045](https://doi.org/10.1146/annurev.aa.26.090188.001045)
- Tomisaka, K. 1984, *PASJ*, 36, 457
- Vázquez-Semadeni, E. 1994, *ApJ*, 423, 681, doi: [10.1086/173847](https://doi.org/10.1086/173847)
- Vázquez-Semadeni, E., Ballesteros-Paredes, J., & Klessen, R. S. 2003, *ApJL*, 585, L131, doi: [10.1086/374325](https://doi.org/10.1086/374325)
- Vázquez-Semadeni, E., Passot, T., & Pouquet, A. 1995, *ApJ*, 441, 702, doi: [10.1086/175393](https://doi.org/10.1086/175393)
- Vázquez-Semadeni, E., Ryu, D., Passot, T., González, R. F., & Gazol, A. 2006, *ApJ*, 643, 245, doi: [10.1086/502710](https://doi.org/10.1086/502710)
- Virtanen, P., Gommers, R., Oliphant, T. E., et al. 2020, *Nature Methods*, 17, 261, doi: [10.1038/s41592-019-0686-2](https://doi.org/10.1038/s41592-019-0686-2)
- Wang, K., Testi, L., Burkert, A., et al. 2016, *ApJS*, 226, 9, doi: [10.3847/0067-0049/226/1/9](https://doi.org/10.3847/0067-0049/226/1/9)
- Williams, J. P., Blitz, L., & Stark, A. A. 1995, *ApJ*, 451, 252, doi: [10.1086/176216](https://doi.org/10.1086/176216)
- Williams, J. P., de Geus, E. J., & Blitz, L. 1994, *ApJ*, 428, 693, doi: [10.1086/174279](https://doi.org/10.1086/174279)
- Yan, Q.-Z., Yang, J., Su, Y., Sun, Y., & Wang, C. 2020, *ApJ*, 898, 80, doi: [10.3847/1538-4357/ab9f9c](https://doi.org/10.3847/1538-4357/ab9f9c)
- Yan, Q.-Z., Yang, J., Su, Y., et al. 2021a, *ApJ*, 922, 8, doi: [10.3847/1538-4357/ac214f](https://doi.org/10.3847/1538-4357/ac214f)
- Yan, Q.-Z., Yang, J., Sun, Y., et al. 2021b, *A&A*, 645, A129, doi: [10.1051/0004-6361/202039768](https://doi.org/10.1051/0004-6361/202039768)
- Yan, Q.-Z., Yang, J., Su, Y., et al. 2022, *AJ*, 164, 55, doi: [10.3847/1538-3881/ac77ea](https://doi.org/10.3847/1538-3881/ac77ea)
- Yuan, L., Yang, J., Du, F., & Su, Y. 2022a, The ^{12}CO and ^{13}CO lines data of 18,190 molecular clouds from the MWISP CO survey, V1, Science Data Bank, doi: [10.57760/sciencedb.j00001.00427](https://doi.org/10.57760/sciencedb.j00001.00427)
- Yuan, L., Yang, J., Du, F., & Yang, S. 2022b, On the Spatial Distribution of ^{13}CO structures within ^{12}CO molecular clouds, V1, Science Data Bank, doi: [10.57760/sciencedb.06653](https://doi.org/10.57760/sciencedb.06653)
- Yuan, L., Li, G.-X., Zhu, M., et al. 2020, *A&A*, 637, A67, doi: [10.1051/0004-6361/201936625](https://doi.org/10.1051/0004-6361/201936625)
- Yuan, L., Yang, J., Du, F., et al. 2021, *ApJS*, 257, 51, doi: [10.3847/1538-4365/ac242a](https://doi.org/10.3847/1538-4365/ac242a)
- . 2022, *ApJS*, 261, 37, doi: [10.3847/1538-4365/ac739f](https://doi.org/10.3847/1538-4365/ac739f)